TECHNICAL NOTE

D-1560

LOW-POWER TESTS OF THE PLUM BROOK REACTOR

By Harold W. Giesler, Harry J. Reilly,
and William A. Poley

Lewis Research Center
Cleveland, Ohio

NATIONAL AERONAUTICS AND SPACE ADMINISTRATION

WASHINGTON

February 1963

NATIONAL AERONAUTICS AND SPACE ADMINISTRATION

TECHNICAL NOTE D-1560

LOW-POWER TESTS OF THE PLUM BROOK REACTOR

By Harold W. Giesler, Harry J. Reilly,
and William A. Poley

SUMMARY

13182

The initial criticality and subsequent low-power tests of the NASA Plum Brook Reactor core are described. Results of control-rod calibrations, flux mapping, and other measurements are given.

The minimum critical size core was found to consist of 11 elements in a 3 × 3 + 2 lattice containing about 1.78 kilograms of uranium 235. The cold clean 3 × 9 core with 168-gram elements had an excess reactivity of 12.0 percent. The maximum differential reactivity worth of the bank of five fueled shim-control rods was measured to be about 2 percent reactivity per inch, and the total worth of each automatically controlled regulating rod was not more than 0.6 percent reactivity.

The reactor temperature coefficient was an average of -0.0075 percent reactivity per ^{o}F over the range 70^{o} to 170^{o} F. The void coefficient was -0.25 percent reactivity for each percent moderator void, for up to 8 percent total moderator void.

Thermal neutron flux traverses of the core indicated the highest fluxes to be in elements LB-6, LC-6, and LD-6, and that the flux peaking increased about 50 percent as the rods were inserted halfway into the core. The relative distributions and the magnitudes of the fluxes were also determined, both in the core and outside the core.

Gamma heating measurements were made, and some of the results are shown.

INTRODUCTION

The Plum Brook Reactor is a 60-megawatt MTR-type testing reactor located at the NASA Plum Brook Station, near Sandusky, Ohio. The reactor facility will be used for the investigation of materials and components for application in spacecraft utilizing nuclear energy. The test facilities include beam-tube and through-hole facilities for irradiation experiments; a complete hot laboratory is also part of the facility. The facility is described in detail in an unpublished NASA report, the "Final Hazards Summary, Plum Brook Reactor Facility," by A. B. Davis, B. Lubarsky, and T. M. Hallman, December 1959 (vols. 1 and 3).

The reactor is the main research tool of the facility. The reactor core (see figs. 1 and 2) consists of a 3 × 9 lattice of MTR-type fuel elements,

cooled and moderated by light water at an inlet pressure of about 160 pounds per square inch absolute. The cooling is by forced circulation, with heat given up to a secondary system. Total initial core loading is 4.4 kilograms of uranium 235 in a volume of about 100 liters, and the design power level is 60 megawatts of thermal power.

The reactor was taken critical for the first time on June 14, 1961. During the next several months a series of tests was performed at power levels below 500 watts and without coolant flow or pressurization to determine the nuclear characteristics of the reactor. These tests included the initial criticality, control-rod calibrations and other reactivity measurements, and thermal neutron flux mapping of the core and the reflector.

This report describes the testing that was done. Not all the results are included here, but the more significant ones are described. The tests are discussed in approximately the sequence in which they were performed, except that they are divided into two major sections, with reactivity measurements in one section and flux measurements in the other.

DESCRIPTION OF REACTOR CORE

The operating core consists of a 3 × 9 lattice of uranium-aluminum fuel elements. The fuel elements have 168 grams of uranium 235 each and consist of fuel plates with uranium - aluminum alloy fuel cores of 16 weight percent uranium at 93-percent enrichment. The fuel core in each plate is 0.020 inch thick by 2.45 inches wide by 23.1 inches long and is clad by 0.020 inch of 1100 aluminum alloy. The plates are curved for strength with a 6-inch radius, and there are 18 plates per element with a center-to-center spacing of 0.175 inch. The plates are brazed into aluminum sideplates, which form two sides of an element. The end fuel plates form the other two sides. The pitch of the lattice is approximately 3.1 inches and the average metal-to-water volume ratio of the fueled core is about 0.75.

The control-rod locations in the core have water-filled cadmium box sections that are removed by being driven upward. All drive equipment is located below the core. The cadmium sections in the fueled core have removable fueled followers, which are similar to the regular elements except that they have only 14 fuel plates and contain approximately 131 grams of uranium 235 each. The two end plates are unfueled, and the two center plates are replaced by a tie plate used to engage or disengage the two sections of the rod. The control rods in the reflector have beryllium followers.

Eight of the 10 control rods are driven by electric motors. Gravity scram actions are provided. The regulating rods at LA-2 and LA-10 (fig. 2) are motivated by hydraulic systems and are used for automatic control.

As can be seen in figure 2, the core is ordinarily to be a 3 × 9 lattice, with beryllium pieces in the LA column and in rows 1 and 11. The lattice at the right in the figure is also composed of beryllium pieces, with a lattice pitch of about 4.3 inches. A large horizontal through-hole test facility, HT-1, goes through this lattice. There are additional test facilities at the north and

south faces of the core. The cooling water enters at the bottom of the tank and passes upward around and through the larger reflector and thermal shields; then the water passes downward through the 4 × 11 lattice.

The operation of the reactor is to be with beryllium rods withdrawn, and the fuel shim rods in a bank to control. One of the regulating rods will be withdrawn, the other used for automatic control. Experiments will be placed in HT-1 and HT-2, in removable cylindrical plugs in the beryllium pieces, and in the beam tubes. However, for the low-power tests, the horizontal beam tube and through-hole facilities were filled with water, except when measurements of the reactivity worth of these facilities were being made.

REACTIVITY MEASUREMENTS

The purpose of the reactivity measurements was to determine the effects of system components on the nuclear behavior of the core. This was necessary to provide information for use in operation of the reactor and to verify the values of reactivity coefficients that were used in hazards analyses of the reactor.

The following discussion first describes the buildup to the initial critical configuration, and the loading from that configuration to the operating 3 × 9 lattice; then the control-rod calibrations are described. Finally, the statistical weight mapping and the temperature and void coefficient measurements are given.

Initial Criticality

Additional instrumentation had to be used for the low-power tests to give sufficient accuracy at the flux levels involved. Two BF_3 counting tubes were installed near the core and connected to scalar counting channels to give source indication at very low fluxes. A linear channel and a log N and period channel were provided. The log N flux and linear flux were recorded on strip charts. A 12-curie polonium-beryllium neutron source was placed in a tube that ended in position RA-2 (see fig. 3). The source was driven by a Teleflex cable, controlled from the Reactor Control Room (RCR). All instrument readouts were in the RCR, giving complete control from that point. Scrams were provided from the linear flux, log N flux, and period.

After the special low-level instrumentation had been checked out for indication of neutron flux at source levels in the core without fuel, the core was prepared for the initial minimum critical assembly.

The core was loaded in steps. In the first step, LC-2, LC-3, and LC-4 were inserted; then LB-3 and LD-3 were added. After that one element was added at a time. At each step the multiplication of source neutrons was measured over the full travel of the control rods. The core was kept surrounded by beryllium pieces at each step. (The pieces from the 4 × 11 lattice are interchangeable.) Figure 3 shows the order of addition of elements, the final configuration for the minimum size critical core, and the locations of special instrumentation.

The inverse multiplications for each channel are shown in figure 4. The values shown are those for the all-rods-out case. The curves indicate a minimum critical loading of about 1715 grams. The smallest core capable of criticality was a 3 × 3 + 2, as shown in figure 3. The excess reactivity of this core was determined to be about 0.50 percent $\Delta k/k$ from period measurements on the shim rods. When the BF_3 counting tube was removed from LA-5 and replaced with a beryllium plug, the excess reactivity increased to about 1.0 percent.

Neutron flux measurements were made to determine the approximate power level of the core for power calibration of the low-level instrumentation. The core was then loaded to the operating 3 × 9 configuration. One row of elements was completed at a time, and measurements of the withdrawal of fueled control rods moving together as a bank to give criticality were conducted for each row. Figure 5 shows the critical bank height as a function of core loading.

The rod positions discussed in this report are given in all cases as indicated rod position in inches. Actually the cadmium withdrawal from the fueled core bottom is less than this. The fuel in a control rod is even with the rest of the core when the rod is at an indicated 30.9 inches. The fuel cores are 23.1 inches long, and there is a 2.2-inch water gap above the fuel core in the rods. Therefore, the cadmium withdrawal from the fuel core bottom is 5.6 inches less than the indicated rod position.

Control-Rod Calibrations

The control rods in the core were calibrated by two different methods. The first consisted of measurements of critical bank height on the fuel shim rod bank for the core with different amounts of uniformly distributed natural boron. The second method was the rod bump-period technique, done in the core with several different boron loadings.

The natural boron was in the form of boron-impregnated polyethylene strips. These were of a size 0.050 inch thick by 0.95 inch wide and of such a length that one end just reached the core bottom while the other end was attached to an aluminum holding piece resting on the top of the fuel plates. The loading of the strips was approximately 1.0 weight percent natural boron, giving a thermal cross section of 6.20 ± 0.20 cm^2 (Maxwellian) per strip over the active core length, assuming a thermal cross section of 762 barns per atom at 2200 m/sec for boron (ref. 1). The boron content of the strips was verified by analytical chemistry and by danger coefficient measurements in an unreflected cylindrical critical assembly at the Lewis Research Center.

The reactivity worth of the strips when distributed among the coolant channels in the fuel elements was computed from the expression

$$\rho = \frac{\Sigma_p}{\Sigma_c + \Sigma_p} \tag{1}$$

(Symbols are defined in appendix A, and the derivation of this expression is given in appendix B.) The self-shielding of the strips was determined by a flux

perturbation cell calculation using a one-group one-dimensional approximation to the thermal flux. This indicated a 3- to 6-percent reduction in the effective cross section of the boron, depending on the number of strips in the core.

The critical bank height of the fuel shims was measured with different numbers of strips in the core. The result of this measurement is shown in figure 6, which is a plot of ρ against H by this method. The number of strips used ranged from zero (clean core) to 250. It was found that the core would be just critical with all rods out when about 188 strips were in the core.

In the rod-bump period measurements, reactivity was related to period by the in-hour equation (ref. 2, p. 301). This equation was used in the "dollars-and-cents" form, which gives reactivities in units independent of the delayed neutron fraction:

$$\rho(\text{cents}) = 100 \sum_i \left(\frac{F_i}{1 + \lambda_i T} \right), \quad F_i \equiv \frac{\beta_i}{\sum_i \beta_i} \tag{2}$$

A value of 0.0064 was used for the delayed neutron fraction (ref. 3). The effect of the greater leakage of prompt neutrons from the reactor was corrected for by use of an "effective delayed neutron fraction," which was calculated by two-group theory to be 1.15 times the delayed neutron fraction, that is, 0.0075. No correction was made for the contribution of delayed photoneutrons, as their effect was believed to be small for this system (ref. 4). The results justified the assumption, as will be seen.

The measurements were performed by placing the reactor critical with the fuel shim rod bank level and then bumping the bank out a given amount and recording the flux on the log N chart for a number of e-folding times. The period was then determined from the log N trace. (This was done by use of a "period protractor" (fig. 7), which utilized the known and constant chart speed and the in-hour equation to interpret the angle of the trace line as equivalent period and reactivity. Use of this device greatly reduced the computational work involved in the measurements.) Then the reactivity was divided by the bank displacement to give the differential rod worth at that height.

The bank rod worth was measured by this method for the clean core and for a number of poisoned cores. This gave a check on the results of the distributed poison measurement. The good agreement between the results by the two methods can be seen in figure 8.

The measurements by the distributed-poison method indicated a total excess reactivity of 12.0 percent $\Delta k/k$. The excess reactivity by the period method was 11.5 percent $\Delta k/k$, computed by the expression

$$\rho_T = 1 - \prod_i (1 - \rho_i) \doteq 1 - \exp(-\Sigma_i \rho_i) \tag{3}$$

These values indicate a K_{eff} of about 1.135 for the clean core with rods out. Calculations presented in the "Final Hazards Summary" (vol. 1, p. 139) had predicted a K_{eff} of about 1.15 or 1.16 for this core. The difference is believed to be due to the influence of the large through-hole, HT-1, on the reflector effectiveness.

The total bank worth of the three beryllium shim rods was measured to be 5.5 percent $\Delta k/k$ by comparison with the fuel shim rods.

The regulating rods were calibrated over their full travel in the clean core, the fully poisoned core, and a "half-poisoned" core. The results for the clean core for one regulating rod are shown in figure 9. The total worth was not more than 80 cents (0.6 percent $\Delta k/k$) at all heights of the fuel shim rod bank; this value is within the 1-dollar maximum worth allowable for these rods.

An additional measurement was that of "stuck rods." It was shown that the reactor was subcritical with one fuel shim rod fully withdrawn when the other fuel shim rods were fully inserted. Also, with the beryllium shim rods inserted, the reactor was subcritical with any three of the fuel shim rods inserted.

Statistical Weight Mapping

Measurements were made to determine the absolute magnitude and the distribution among lattice locations of the fuel and poison statistical weights. This was done to determine the reactivity worth of fuel and poison when inserted at various points into the reactor. The method was to measure the control-rod bank height of the fuel shim rods in the clean core with reference loading, and then replace one element with a modified element and again measure the bank heights. The change in bank height thus measured was used to compute the reactivity worth of the change from the standard element to the modified element. Half of the lattice was mapped in this way, with a check at one location on the other end to verify symmetry.

The modified element for the fuel statistical weight mapping was an element having 14 fueled plates and four unfueled plates, but otherwise identical to the other elements. The modified element for poison weight mapping was a standard element with eight boron strips added to the element. Therefore, the change in fuel loading or boron loading at each lattice location was known, so that the worth per gram of change in loading could be computed.

The results of these measurements are shown in table I. The distributions of the statistical weights for fuel and poison are normalized to a maximum of unity. The average value of the absolute magnitude is shown. The removal of fuel or the addition of poison to the core introduced negative reactivity for all cases considered. The measured core average statistical weights agree within ±10 percent with values calculated from a simple modified four-factor analysis.

Temperature Coefficient

The reactivity temperature coefficient was measured over the range 70° to 170° F. The heating of the system over this range was accomplished by running the primary main pumps while maintaining zero flow in the secondary system. This gave a nearly constant heating rate of about 10° F per hour, which provided adequate times to perform measurements while heating up. Measurements were also taken while cooling down, which was accomplished by running the shutdown main pumps, with intermittent flow in the shutdown secondary system. This gave cooling in steps of about 10° to 15° F. Measurements were taken after each step decrease in temperature.

The temperature of the water in the core was determined by two thermocouples read out on a millivolt potentiometer. One of these thermocouples was attached to the source tube at a location about 1 foot above the core; the other was one of the sensors installed in an instrumentation tube ending about 5 feet below the core. In this way it was possible to determine moderator temperatures within ±1° F and temperature changes within ±0.1° F. Temperatures were measured about every 5 minutes throughout the test.

The reactivity changes caused by the temperature increase were found by measuring the critical bank height at different temperatures while heating. The method used during heating was to place the reactor slightly supercritical at a given bank height and then allow the temperature to "catch up" with the reactor, making it subcritical after a time. This made it possible to determine the time of criticality within about ±1/2 minute. During cooling down, the temperature was almost constant after each step decrease in temperature so that the critical height was determined directly.

Since the temperature and rod position were known as functions of time, it was possible to determine the rod position as a function of temperature. The rod positions were then corrected for expansion effects and for a core deflection effect due to the pressure drop across the core when the pumps were on. The data (corrected rod position against temperature) were correlated by a second-order polynomial least-squares fit, giving the equation

$$Y = 0.2006 + 0.0541\ X + 0.1336\ X^2 \qquad (4)$$

where

Y rod position in inches above 15 in.

X temperature, hundreds of °F

This equation was differentiated to obtain the change in rod position due to a change in temperature at each temperature. The rod worths at each rod position were taken from the control-rod calibrations, giving the temperature coefficient at each temperature. The temperature coefficient is plotted in figure 10. The total temperature defect over the range 70° to 170° F was found to be about 1 dollar (0.75 percent $\Delta k/k$) by integrating the curve of figure 10. These values are in good agreement with the values calculated in the "Final Hazards Summary" (vol. 2, p. 8) within the accuracy of the measurement.

Void Coefficient

The core void coefficient for uniformly distributed voids was measured by placing numbers of magnesium strips among the fuel elements and measuring the critical bank height for each case. The assumption was made that the magnesium was equivalent to 90 percent void (ref. 5). Measurements were made with up to 10 void strips per element, or up to 8.15 percent of core moderator volume voided. The void coefficient was determined to be approximately -0.25 $(\Delta k/k)/(\Delta v/v_{mod})$, and was almost linear with void volume over the range measured.

The distribution of void coefficient among elements was mapped in a manner similar to that of the statistical weight mapping experiments. The void coefficient ranges from a maximum of $-0.49(\Delta k/k)/(\Delta v/v_{mod})$ at LC-5 to a minimum of $-0.08(\Delta k/k)/(\Delta v/v_{mod})$ at LD-2. The distribution of void coefficient is shown in table II.

The effect of voiding flooded test holes was measured in the clean core. Reactivity worths were determined by measurement of the displacement of the fuel shim critical bank height. Worths of individual test holes HT-1 and 2 and HB-1, 2, and 3 were measured, and combinations of these were also measured for possible interaction effects. Voiding introduced negative reactivity in all cases. HB-1, 2, and 3 were worth less than -2 cents each; HT-1 was worth -61 cents; and HT-2 was worth -38 cents. There was no measurable interaction between holes.

These measurements clearly indicated the large reactivity worth of the through-hole facilities; the measurements also verified the calculations of the "Final Hazards Summary" (vol. 2, p. 138), which predicted that voiding any facility would introduce negative reactivity to the core.

NEUTRON FLUX MEASUREMENTS

It was necessary to measure the spatial distribution of fission power in the core, as a function of banked rod position, in order to determine the reactor heat transfer during operation at full power. It was also necessary to determine the absolute magnitude of the thermal flux in the core so that the low-power instrumentation could be calibrated for power level. Measurements of thermal flux in the reflector and test facilities were made to provide some information on what could be expected in these regions.

The discussion that follows first describes the core power-distribution measurements, as they were made by a method utilizing a new fission-probe instrument and by a standard method. Then the core power-calibration is given, followed by the reflector flux-mapping measurements.

Core-Power Distribution Measurements

Basically, two methods of mapping the core were available. One method utilized an automatic flux plotter device, which has uranium 235 coated semiconductors as sensing elements; the other consisted of the usual foil irradiation and counting techniques.

The automatic flux plotter is described in detail in reference 6. It has scalar counters and print-out and monitoring equipment in a console assembly, while the probe instrument itself (fig. 11) is placed down on top of the core. The probe instrument has four probes which are driven simultaneously between the fuel plates of an element. Each probe has on its end a semiconductor consisting of a silicon p-n junction wafer coated with uranium at 93-percent enrichment. At low flux levels the output of each semiconductor is proportional to the fission flux; the output for each probe is automatically printed out at the console on paper tape, along with probe number and vertical position from the top of the fuel plates on which the instrument rests. Counts can be recorded at any spacing desired, but 1/2- and 1-inch space intervals were used for the tests. The counting channel cycles from one probe to another, taking counts for a time-interval and pausing for an interval, while the probes are moving. All these time intervals are of adjustable length. Figure 11 shows a schematic representation of the probe instrument when in place in the core. Note that it can be moved from one element to another easily and quickly. However, it does not fit into control-rod elements.

Irradiation measurements utilized gold wires, both bare and cadmium-covered. The wires were 0.50 inch long and 0.030 inch in diameter. The cadmium covers were made from tubing having 0.020-inch wall thickness.

The wires were taped to Lucite wands, which fitted between the fuel plates. These wands were about 1 inch wide, 0.080 inch thick, and when inserted extended the length of the core. The wands were designed to hold either foils or wires, with or without cadmium covers, spaced as closely as 1-inch intervals in either direction from the core centerline. In all cases, except measurements for local peaking effects, wands were inserted nearer the south side of each row than the north side because each element has a "comb" at each end of the fuel plates (see insert in fig. 12), which prevented the wands from being in the middle of the element. Therefore, the wires were about 1 inch from the south side of an element and 2 inches from the north side in all measurements except those for local peaking effects.

Determination of relative flux distribution from wire measurements was facilitated by an automatic sample counting and changing machine. This system effectively related the beta activity of each irradiated wire to a single wire (from that irradiation) used as a monitor for a fixed number of counts on the monitor in each case. This obviated any need for decay corrections. Most of the uncertainties in flux perturbation and other effects also cancel out when determining relative flux distribution.

Also available for the flux measurements were boral strips containing 1.1 weight percent natural boron in aluminum. These allowed poisoning of the core to attain any desired critical bank height for flux measurements. About 60 of these strips were sufficient to poison the core fully.

Most of the wire irradiations were done at a reactor power of 300 watts, which was necessary to give good counting statistics on the activated wires. The flux plotter was used at a reactor power of less than 10 watts. This was the

lowest power level that gave acceptable counting statistics for the flux plotter and was chosen because of the limited lifetime of the semiconductor detectors in an irradiation field.

Model Used for Synthesis of Power Distribution

The measurements were designed to produce a representation of the power distribution in the reactor core at different times during the reactor cycle. It was believed that the flux distributions would be primarily dependent on the control-rod bank positions and that power distribution would essentially follow the thermal flux distribution. The uniform loading of fuel at a rather low density and the low absolute depletion during a cycle justified these assumptions. It was decided that the fission probe device gave a very accurate measurement of the power distribution in the clean core, especially in regard to the average power per element and the vertical flux shape per element. This was used as the reference case. Then a simpler model was used to synthesize the power distribution in the clean core and in several poisoned cores, and the validity of this model was tested by comparison with the reference case.

For the reference case, all 22 fixed elements in the clean core (rods at 15.4 in.) were mapped with the automatic flux plotter. Several elements in a poisoned core (rods at 22.2 in.) were also mapped with the automatic flux plotter. Counts were taken on each probe at 1/2-inch intervals in the clean core and 1-inch intervals in the poisoned core.

Bare and cadmium-covered gold wires were irradiated in the control rod at LC-6 to get an accurate estimate of the flux distribution in control rods. Also, a number of interelement horizontal traverses were performed to determine the local peaking effects of sideplates, control rods, water gaps, and reflectors. These were done with bare and cadmium-covered gold wires, and sufficient mapping was done to relate any point in an element to the element average.

The method used to synthesize three-dimensional power distributions throughout core life was as follows:

(1) Bare gold wires were irradiated in the core with critical bank heights of 15.4, 18.3, 22.3, and 27.8 inches.

(2) At each bank height, vertical traverses were performed in elements LB-6 and LD-6 using wires at 2-inch intervals in each traverse. Also, wires were irradiated at an elevation of 6 inches below the core centerline (-6 in.) in LB-2, 4, 5, 8, 9, and 10 and in LD-5. Cadmium-covered wires were irradiated in LB-3 and 7 and LD-7 for additional information.

(3) It was assumed that the relative vertical flux distribution in all elements in the LB row was the same as that in LB-6, that the LD row followed LD-6, and that the LC row (fixed elements) resembled the LB row. The relative horizontal distribution in the east-west direction was assumed to be the same for all rows, and the measurements at -6 inches were used to predict this distribution.

(4) No measurements were performed in the control-rod fuel sections for the synthesis. For the control rods, it was assumed that the relative vertical flux shape in the portion of the fuel section of LC-6 that was in the core had the same shape as the adjacent portion of LB-6. The correct magnitude was obtained from the interelement traverses made in the clean core. A local peaking effect was superimposed at the top of the fuel, where there is a metal-water volume in the control rod, using the results of the clean core measurements. It was assumed that the flux in the control rod tapered off in an exponential fashion below the core. The horizontal east-west distribution in the LB row was used to predict the fluxes in the other control rods.

Results

The power distribution synthesized by the model for the clean core showed agreement within ±5 percent at all points with the automatic flux plotter results for the clean core. The synthesized control-rod powers were 5 percent low compared with the reference case. This was corrected for in the heat-transfer analysis.

Cadmium ratio measurements indicated that the epicadmium activity in the active core was from 25 to 35 percent of the total bare gold activity. The cadmium ratio changed continuously near the top and bottom of each vertical traverse, so that it was difficult to correct the bare gold traverses to subcadmium traverses. Work performed indicated that the subcadmium traverses, when normalized to core average, agreed with the normalized bare gold traverses within about ±5 percent at all points. Therefore, it was assumed that the thermal flux distributions were approximated by the bare gold distributions.

The results of these measurements are summarized in table III and figures 12 to 18. In the figures, power is given relative to the core average along the ordinate, and position is given as the distance above the core centerline along the abscissa. Core centerline is taken to be at the imaginary horizontal plane midway between the top and bottom of the fueled core. Positions below core centerline are expressed as negative numbers on the abscissa (e.g., -6 in.).

Figure 12 shows a traverse by the automatic flux plotter in element LB-6 for the clean core. The individual probe results are shown. Figure 12 also shows where the probes are located in an element when in use. Note that probe 1, which in this case is closest to control-rod LC-6, has a lower flux than the others in the upper part of the traverse, which is adjacent to the partially inserted control rod. Probe 3 is nearest the reflector and shows as an increased flux over the whole length of the traverse.

Table III summarizes the power distribution among elements for all measurements. Note the discrepancy between the values in control rods by the two methods. Also, the power distribution measured by the automatic flux plotter in the poisoned core shows a slightly different trend with rod withdrawal than do the wire measurements. This trend is believed to be due to the fact that the boral strips could not be distributed uniformly for the fission plotter measurement, leading to secondary flux perturbation effects.

Figure 13 shows one of the vertical traverse measurements in control-rod LC-6 for the clean core. Figure 14(a) shows the way the model synthesized this traverse. Figure 14(b) shows the vertical traverse measurement in element LD-6 by bare gold and by the automatic flux plotter in the clean core. Note that the bare gold values are higher at the top of the core and lower at the bottom than are the fission flux values. However, this effect was just the opposite in element LB-6, because the bare gold traverse was closer to the control rod than the traverse in LD-6, while the fission probe traverse was relatively the same.

Figures 14 to 17 show the traverses for LC-6 and LD-6 at each bank height, as synthesized by the model. The flux distributions are very dependent on rod position; also, the flux distribution in a control rod is very different than that in a fixed element when the rods are inserted. The measurements for the case with rods at 27.8 inches show good agreement with the calculations of the "Final Hazards Summary" for the rods-out case, as would be expected.

Quite a few measurements were made on interelement local peaking effects, but it is not of interest to discuss them all. Figure 18 shows the thermal flux for a traverse across the core at an elevation of 7 inches below the core centerline, which elevation is below the control rods. The values obtained from the fission probes at this level are also shown.

The measurements allowed construction of the power distribution in the core at several times during depletion. The accuracy was estimated to be in the neighborhood of ±20 percent at each point at a confidence level of 95 percent.

Approximate Power Calibration

An approximate power calibration of the core was made early in the test series. A total of 74 bare and cadmium-covered gold foils (0.25 in. diam. by 0.005 in. thick) and wires (0.50 in. long by 0.030 in. diam.) were irradiated in one run at constant power. The data points included vertical traverses of LB-6 and LD-6 with foils and wires, respectively, at 1-inch intervals from the core centerline. The other data points were at 0 and -6 inches from the core centerline in the even-numbered locations in the LB and LD rows and the odd-numbered locations (fixed elements) in the LC row.

A number of assumptions were made in determining core power from the measurements. First, it was assumed that the flux perturbation effect (depression plus self-shielding) was the same for wires as for foils. The value used for foils was 0.86, based on measurements that had previously been performed at the critical assembly mentioned on page 4. Second, it was assumed that the horizontal flux distribution in the core was symmetric about the north-south axis and the vertical flux distributions in fuel sections of shim rods were the same as in the fixed elements. Finally, it was assumed that the thermal flux spectrum in the core followed a Maxwellian distribution, so that the subcadmium activation rate of the detectors was proportional to Maxwellian thermal flux times Maxwellian thermal absorption cross section corrected for temperature. However, the 2200 m/sec cross section for gold was used to derive the 2200 m/sec fluxes; then these fluxes were used with the 2200 m/sec cross section for uranium 235 to give the specific power. Epicadmium activities calculated from cadmium-covered foils

were multiplied by the value 1.013 to correct for epicadmium absorptions in the cadmium covers. No correction was made for leakage of thermal neutrons through cadmium covers, because it was calculated that this leakage was negligible for the thicknesses involved.

The foils and wires were counted on a beta-gamma coincidence counter and then corrected for decay to determine absolute activity at shutdown of the reactor. The equation used to determine activity at time t after shutdown was (ref. 7, pp. 320-328):

$$A(t) = \frac{(C_1 - B)(C_2 - G)}{\left[C_3 - (C + 2\tau C_1 C_2)\right]} \tag{5}$$

From this the activity at shutdown was determined by the following equation (ref. 8, p. 53):

$$A(o) = \frac{A(t)}{\left[1 - \exp(-\lambda t_e)\right]\left[\exp(-\lambda t_w)\right]} \tag{6}$$

for both bare and cadmium-covered foils and wires. The thermal flux was determined from equation (6) by the equation

$$\Phi_{th} = \frac{A_b - 1.013\, A_{cd}}{60(0.86)\sigma_a N_T} \tag{7}$$

where the values 1.013 and 0.86 are the corrections mentioned previously.

Equations (5) to (7) allowed determination of the average flux in the reactor during the irradiation. To obtain core power from this flux, the equation used was:

$$P' = \frac{eN_o\sigma_f M \Phi_{th}}{A} \tag{8}$$

(where A is the atomic weight for uranium 235, 235 g/g-mole) which reduces to

$$P(\text{watts}) = 4.82\times10^{-11} \sum_i M_i \bar{\Phi}_i \tag{9}$$

assuming 196.7 Mev per fission and 1.602×10^{-13} watt-seconds per Mev, giving an expression for power when flux is given.

The reactor power during the run was determined by these methods to be 16 watts, within a probable error of about ±20 percent. This allowed power calibration of the low-power instrumentation, and this calibration was used throughout the tests.

Flux Mapping in Core, Reflector, and Test Facilities

Bare and cadmium-covered gold wires and bare dysprosium foils were used to determine thermal neutron flux in the core and the reflector. The gold wires, cadmium covers, and lucite flux wands used were the ones described previously. The dysprosium foils were 4.8 percent dysprosium and 95.2 percent aluminum of 0.25-inch diameter and 0.006- or 0.007-inch thickness, and were used principally for determination of thermal fluxes in beryllium L pieces. (These pieces have limited space for detectors, allowing use of bare gold wires but not cadmium-covered wires.)

In addition to the lucite wands used in the core, aluminum wands were used in the beryllium R pieces. These pieces have 3/16-inch holes drilled vertically into their corners. The aluminum wands were rods of 0.129-inch diameter with slots milled at various locations along their lengths. Detector wires were inserted into the slots, and the rods were placed into the R pieces for irradiation. For the L pieces, the dysprosium foils and bare gold wires were taped to the sides of the removable center plugs for irradiation.

For the test facilities, HT-1 and 2, and HB-1, 2, and 3, special devices were constructed of lucite to position the detector materials properly. These devices consisted of lucite rods on which movable lucite wands were mounted like spokes on a wheel with the rod being the shaft. In this way it was possible to place detector materials at any location desired within the test holes.

The measurements included gold wire irradiations at the horizontal midplane and at 4 inches above and 4 inches below the horizontal midplane. This was done as far as possible throughout the core and reflector. (In the R reflector, the presence of the horizontal through-hole HT-1 prevented placement of foils at the 0- and -4 in. elevation in the RA and RB rows.) For the test holes, detectors were placed at various locations along horizontal and vertical diameters of each hole at positions nearest the core and at several positions along the axis of each hole. The irradiations were done with all test holes filled with water.

Count rates on the irradiated detectors were determined by the automatic sample counting and changing system described previously, with each detector counted against the monitor detector. The activation count rates were related directly to the calculated average flux-per-watt value. The thermal flux perturbation for the wires was assumed to be the same for the wires whether irradiated in the core or outside the core. The true perturbation effect was probably greater in the reflector than in the core. The effect of this assumption was to introduce no error in calculating core power level but to cause some underestimate of true thermal flux outside the core.

It was calculated from the results of the core-power distribution measurements that 90 percent of total clean core power was generated in the fixed fuel elements, so that $\overline{\Phi} = 5.03 \times 10^{6}$ n/cm^2-sec-watt for the 168-gram elements, based on equation (9).

The flux 4 inches below the core centerline (-4 in.) in LB-7 was measured to be 1.93 times the core average, so that at this location $\Phi = 9.71 \times 10^6$ $n/cm^2/sec/watt$. The subcadmium activity at this location was measured to be 9.60×10^4 counts per second. Division of the calculated flux as this point by the activity measured gave a value 1.01×10^2. This factor was used to relate all subcadmium activations in and outside the fueled core to true thermal flux per watt.

Some of the results of the measurements are summarized in figures 19 to 22. Figure 19 shows thermal flux per watt at the 4-, 0-, and -4-inch elevation from the core centerline going in the north-south direction across the core and through the reflector. Figures 20 and 21 show thermal flux per watt along the axes of HB-2, HT-1, and HT-2. Figure 22 shows an isoflux plot for a horizontal cross section of the core and reflector at 0-inch elevation from the core centerline.

GAMMA HEATING MEASUREMENTS

Measurements of the gamma heating of materials in the reflector and in the vicinity of the test facilities were made using ion chambers and chemical dosimeters.

The ion chambers were constructed of a variety of materials: aluminum, stainless steel, beryllium, copper, and tantalum. The cavities were filled with air. The chambers were designed according to the Bragg-Gray theory (ref. 9, p. 30), which states that: (1) For a very small cavity in a volume of material, the cavity does not affect significantly the radiation spectrum or intensity, and (2) the ratio of the energy dissipation per unit mass of gas to that of the chamber material equals the ratio of mass stopping power of the gas to that of the chamber material. It was assumed that the ratio of the mass stopping powers was a weak function of the energy spectrum, so that an average value could be used. This yielded the equation

$$E_M = \frac{S_M}{S_{air}} J_{air} W_{air} \tag{10}$$

The values S_M/S_{air} used were as follows (ref. 9, p. 30):

Beryllium	0.916
Aluminum	.886
Copper	.775
Stainless steel	.790
Tantalum	.622

This relation enabled calculation of the chamber current produced per unit incident radiation for each chamber. The results of the calculations were verified experimentally by calibration measurements with a cobalt 60 source of known intensity.

In the reactor measurements, dose rates were measured in rads so that no corrections for air equivalence were necessary. Ion chamber currents were measured with electrometers. Positioning of chambers around the core was done with simple cable and clamp devices.

Ferrous sulfate chemical dosimeters (ref. 10) were used to give a comparison with the ion chamber measurements. The ferrous sulfate solution was contained in polystyrene bottles about 3 inches in length and $1\frac{1}{4}$ inches in diameter. The bottles were placed in rubber balloons to contain any leakage and were positioned by the same device as the ion chambers. After irradiation, the optical density of the irradiated solution in a dosimeter was measured by the use of a spectrophotometer. This allowed calculation of the radiation dose rate during the irradiation of the dosimeter.

The measurements performed included horizontal traverses in the beryllium reflectors and vertical traverses with copper ion chambers in positions LA-7 and RD-4. Additional measurements were made in the water around the core. Most of the measurements were made using the aluminum and copper ion chambers; however, in several test positions all the chambers were used. The ion chamber measurements were made in six runs, each of which included irradiations at reactor powers of 10, 50, and 100 watts. Chemical dosimeter measurements were made at a reactor power of 500 watts.

The chemical dosimeter results agreed with the ion chamber results except in the RD row in the reflector, where dose rates were below the range of accuracy of the chemical dosimeters. The absolute accuracy of the ion chamber results was calculated to be about +5 to -15 percent. (The chambers tend to "read high" because of the (n,p) reactions in the chamber material.) Some of the results are shown in figures 23 and 24. Figure 23 shows the gamma heating of the aluminum ion chambers, at a total reactor power of 60 megawatts, along reflector lattice row number 4 at an elevation $7\frac{1}{2}$ inches above the core centerline. Figure 24 shows the vertical traverses of LA-7 and RD-4 using the copper ion chambers. A vertical traverse was not performed in the RA row, but it is expected that the vertical distribution of the heating would be similar there to that of LA-7, as both are about the same distance from the active core.

The results indicate that the gamma heating at the beginning of a cycle will be a maximum of about 18 watts per gram of aluminum at -6 inches just adjacent to the core at RA-4, and 14 watts per gram of copper at -6 inches in the center of beryllium element LA-7. The gamma energy flux appears to be attenuated (fig. 23) in the beryllium with a relaxation length of about 4 to 5 inches. The gamma heating in the active lattice can be expected to be greater, possibly twice as great at the center (LC) row as at comparable locations in the LA row. The heating rate will be about the same for each material, in watts per gram of material (eq. (10)).

CONCLUSIONS

The reactivity characteristics of the reactor in regard to control-rod worth, excess reactivity, fuel and poison worths, and temperature coefficient were measured. The thermal neutron flux, gamma heating, and fission power distribution in and around the reactor were determined. The measurements verified the design calculations of the reactor nuclear parameters; in general, they showed the hazards analysis of the reactor had been conservative in the choice of values of rod worth, reactivity coefficients, and fluxes for use in the analysis. The measurements also indicated that the reactor core nuclear characteristics were acceptable for operation.

Lewis Research Center
National Aeronautics and Space Administration
Cleveland, Ohio, October 3, 1962

APPENDIX A

SYMBOLS

$A(o)$	absolute activity at shutdown, disintegrations/min
$A(t)$	absolute activity at time t, disintegrations/min
A_b	bare detector activity at shutdown, disintegrations/min
A_{cd}	cadmium-covered activity at shutdown, disintegrations/min
B	beta background, counts/min
C	coincidence background, counts/min
C_1	beta counts, counts/min
C_2	gamma counts, counts/min
C_3	coincidence counts, counts/min
E_M	energy lost in chamber material, rads/sec
e	fast fission factor, assumed to be equal to 1.08
G	gamma background, counts/min
H	indicated rod bank position, in. of withdrawal
J_{air}	measured chamber response, amp/cm^3 at STP in chamber air
K_{eff}	effective neutron multiplication factor
k	excess multiplication factor
M	fuel mass, g
M_i	fuel loading per element, g
N_o	6.023×10^{23} atoms/g-mole
N_T	atoms of gold
P'	fission rate, fissions/sec
S_M/S_{air}	average ratio of mass stopping power of chamber material to that of air
T	reactor period, sec
t_e	irradiation time, min

t_w	wait time, min
$\Delta v/v_{mod}$	effective moderator void fraction
W_{air}	energy expended in producing unit charge, 2.80×10^9 rad-cm^3/amp-sec
β_i	delayed neutron fraction, group i
λ	decay probability, min^{-1}
λ_i	decay probability for group i, sec^{-1}
ρ	reactivity, $\Delta k/k$
ρ_i	excess reactivity over increment i
ρ_T	total excess reactivity
Σ_c	total thermal absorption cross section of clean core, cm^2, averaged over Maxwellian spectrum
Σ_p	total thermal absorption cross section of poison, cm^2, averaged over Maxwellian spectrum
σ_a	microscopic activation cross section for gold, cm^2/atom, 2200 m/sec
σ_f	microscopic fission cross section for uranium 235 (ref. 11); 2200 m/sec value is $582 \times 10^{-24} \times 0.98 \times 0.97$ cm^2/atom; last two values are corrections for non-1/v cross section and thermal flux disadvantage factor
τ	resolving time of coincidence counter, min/count
Φ	average thermal flux in core, n/cm^2-sec, at 2200 m/sec
Φ_{th}	thermal flux, n/cm^2-sec, at 2200 m/sec
$\bar{\Phi}_i$	average thermal flux per element, n/cm^2-sec, at 2200 m/sec
$\sum_i$	summation over index i
$\prod_i$	multiplication over index i

APPENDIX B

DERIVATION OF EXCESS REACTIVITY EQUATION

The reactivity effect of insertion of the control rods was considered to be a change in leakage of neutrons from the fueled region, that is, a geometric buckling effect. The effect of insertion of the boron strips into the fuel elements was considered to be a change in thermal utilization in the fueled region.

Thus, for the critical core in the clean condition,

$$K_{eff} = 1 = \frac{n\epsilon p}{1 + M^2 B_c^2} \frac{\Sigma_a^{25}}{\Sigma_c} \tag{B1}$$

where

$\frac{n\epsilon p}{1 + M^2 B_c^2}$ conventional four-factor equation (ref. 2, p. 216) without the thermal utilization term

B_c^2 geometric buckling of clean core

Σ_a^{25} absorption cross section of fuel

Σ_c clean core cross section

Also, for the critical core with boron strips,

$$K_{eff} = 1 = \frac{n\epsilon p}{1 + M^2 B_p^2} \frac{\Sigma_a^{25}}{\Sigma_c + \Sigma_p} \tag{B2}$$

where

B_p^2 geometric buckling of the poisoned core (B_p^2 is different from B_c^2 because of rod position)

Σ_p absorption cross section of poison

From equation (B2),

$$\frac{n\epsilon p}{1 + M^2 B_p^2} = \frac{\Sigma_c + \Sigma_p}{\Sigma_a^{25}} \tag{B3}$$

If the control rods in the clean core are withdrawn to the position of equation (B2), equation (B1) becomes

$$K_{eff} = \frac{\Sigma_c + \Sigma_p}{\Sigma_a^{25}} \cdot \frac{\Sigma_a^{25}}{\Sigma_c} = \frac{\Sigma_c + \Sigma_p}{\Sigma_c} = 1 + \frac{\Sigma_p}{\Sigma_c}$$

If $K_{eff} = 1 + \Delta K$, then

$$\Delta K = \frac{\Sigma_p}{\Sigma_c} \tag{B4}$$

And since

$$\rho \equiv \frac{K_{eff} - 1}{K_{eff}} = \frac{\Delta K}{K_{eff}}$$

then

$$\rho = \frac{\Sigma_p}{\Sigma_c} \frac{\Sigma_c}{\Sigma_c + \Sigma_p} = \frac{\Sigma_p}{\Sigma_c + \Sigma_p} \tag{B5}$$

REFERENCES

1. Anon.: New Cross Section for Boron. Nucleonics, vol. 19, no. 6, June 1961, p. 73.

2. Glasstone, Samuel, and Edlund, Milton C.: The Elements of Nuclear Reactor Theory. D. Van Nostrand Co., Inc., 1956.

3. Moore, K. V.: Tables of Reactivity vs. Period for U^{235}, Pu^{239}, and U^{233}. IDO-16485, Phillips Petroleum Co., Sept. 10, 1958.

4. Fader, W. J., and Harrison, R. C.: The Determination of the Period-Reactivity Relation and Open-Loop Reactor Transfer Function from Rod-Drop Decay Data. Nuclear Sci. and Eng., vol. 11, no. 4, Dec. 1961, pp. 405-414.

5. deBoisblanc, D. R., and Marsden, R. S.: Preliminary Evaluation of the 20 Percent Enriched Uranium Core for the Materials Testing Reactor. IDO-16459, Phillips Petroleum Co., June 3, 1958.

6. Steinberg, R.: Experimental Results of Rapid In-Core Flux-Mapping Techniques in the Plum Brook Reactor. IRE Trans. on Nuclear Sci., vol. NS-9, no. 1, Jan. 1962, pp. 97-104.

7. Bleuler, Ernst, and Goldsmith, George J.: Experimental Nucleonics. Reinhart & Co., Inc., 1952.

8. Dungan, W. E.: Neutron Spectrum Measurements with Radioactivants. ANP. NARF-57-57 T, MR-N-177, Convair Div., General Dynamics Corp., Dec. 30, 1957.

9. Hine, Gerald J., and Brownell, Gordon L.: Radiation Dosimetry. Academic Press, Inc., 1956.

10. Taimuty, S. I.: Recent Developments in Gamma Ray Dosimetry. Materials in Nuclear Applications, ASTM Spec. Tech. Pub. 276, 1960, pp. 9-17.

11. Hogg, C. H.: Thermal Neutron Flux Measurement at the MTR-ETR Site. IDO-16538, Phillips Petroleum Co., Oct. 28, 1960.

TABLE I. - STATISTICAL WEIGHT DISTRIBUTION FOR FUEL AND POISON

[Fuel: Absolute statistical weight at LB-6, 1.13 cents/g uranium 235; core average, 0.69 cents/g. Poison: absolute statistical weight at LB-6, 83.0 cents/g natural boron; core average, 53.0 cents/g.]

Key

N_1
N_2

N_1 = value for fuel

N_2 = value for poison

	LB	LC	LD
2	0.27 .29		0.25 .23
3	0.39 .48	0.42 .52	0.49 .48
4	0.80 .74		0.74 .69
5	0.76 .90	0.99 .99	0.66 .81
6	1.00 1.00		0.80 .84
		0.41 .46	

TABLE II. - STATISTICAL WEIGHT DISTRIBUTION FOR VOIDS

[Absolute statistical weight at LC-5, -65.0 cents/percent moderator void; core average, -36.0 cents/percent.]

	LB	LC	LD
2	0.22		0.16
3	.42	0.46	.48
4	.69		.65
5	.71	1.00	.62
6	.77		.68
7		.89	
8			
9		.43	
10			

TABLE III. - PERCENT POWER GENERATION IN FUEL ELEMENTS

Fuel-element number	Gold data (a)				Fission probe data (b)	
	Rods at 15.4 in.	Rods at 18.3 in.	Rods at 22.3 in.	Rods at 27.8 in.	Rods at 15.4 in.	Rods at 22.2 in.
LB-2	2.76	2.86	2.80	2.77	2.83	2.96
LB-3	3.81	3.79	3.86	3.93	3.75	3.75
LB-4	4.62	4.50	4.62	4.56	4.57	4.39
LB-5	5.11	4.90	4.67	4.64	5.04	5.05
LB-6	5.16	5.01	4.94	4.80	5.17	5.28
LB-7	4.98	4.87	4.72	4.66	5.03	5.14
LB-8	4.46	4.39	4.31	4.19	4.43	4.28
LB-9	3.55	3.54	3.32	3.32	3.63	3.35
LB-10	2.73	2.63	2.68	2.65	2.68	2.59
LC-3	3.64	3.62	3.69	3.74	3.52	3.68
LC-5	4.86	4.64	4.45	4.42	4.73	4.83
LC-7	4.74	4.61	4.50	4.44	4.58	4.92
LC-9	3.37	3.37	3.17	3.15	3.31	3.20
LD-2	2.62	2.83	2.76	2.73	2.68	2.74
LD-3	3.60	3.74	3.84	3.87	3.65	3.48
LD-4	4.37	4.44	4.58	4.48	4.41	4.07
LD-5	4.83	4.81	4.62	4.58	4.88	4.69
LD-6	4.88	4.95	4.87	4.74	4.85	4.89
LD-7	4.72	4.78	4.67	4.60	4.69	4.77
LD-8	4.21	4.30	4.26	4.13	4.14	3.97
LD-9	3.35	3.48	3.27	3.28	3.39	3.11
LD-10	2.58	2.58	2.63	2.58	2.52	2.40
LC-2	1.53	1.70	1.82	2.01	1.65	1.89
LC-4	2.56	2.66	3.00	3.32	2.71	2.81
LC-6	2.87	2.97	3.20	3.48	3.04	3.38
LC-8	2.48	2.58	2.80	3.03	2.56	2.74
LC-10	1.52	1.56	1.75	1.91	1.55	1.66

[a]Synthesized from bare gold irradiations.

[b]Reference case; constructed from fission-probe traverses in fixed elements and wire irradiations in control-rod LC-6.

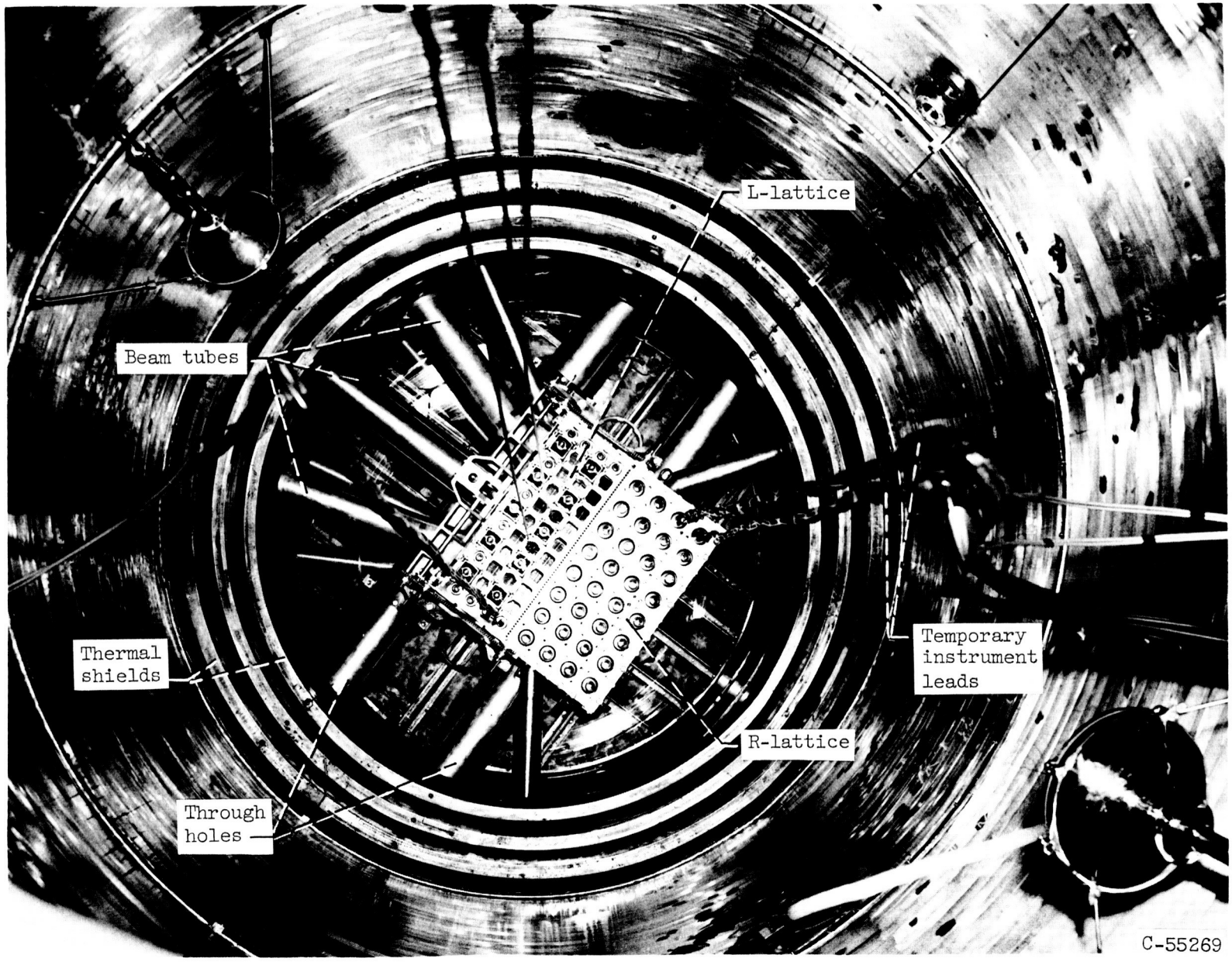

Figure 1. - Reactor core as photographed from tank top.

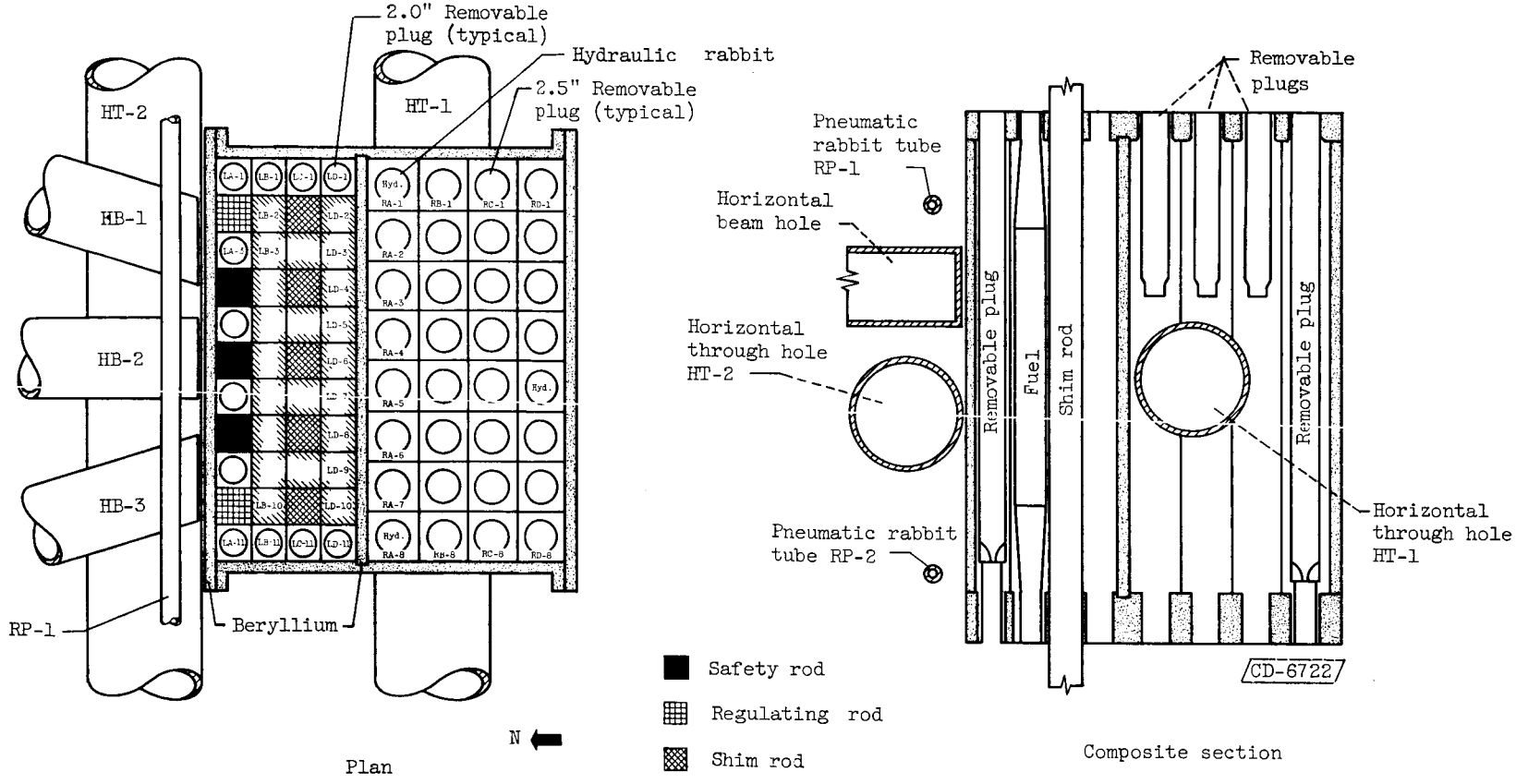

Figure 2. - Reactor core and experimental facilities.

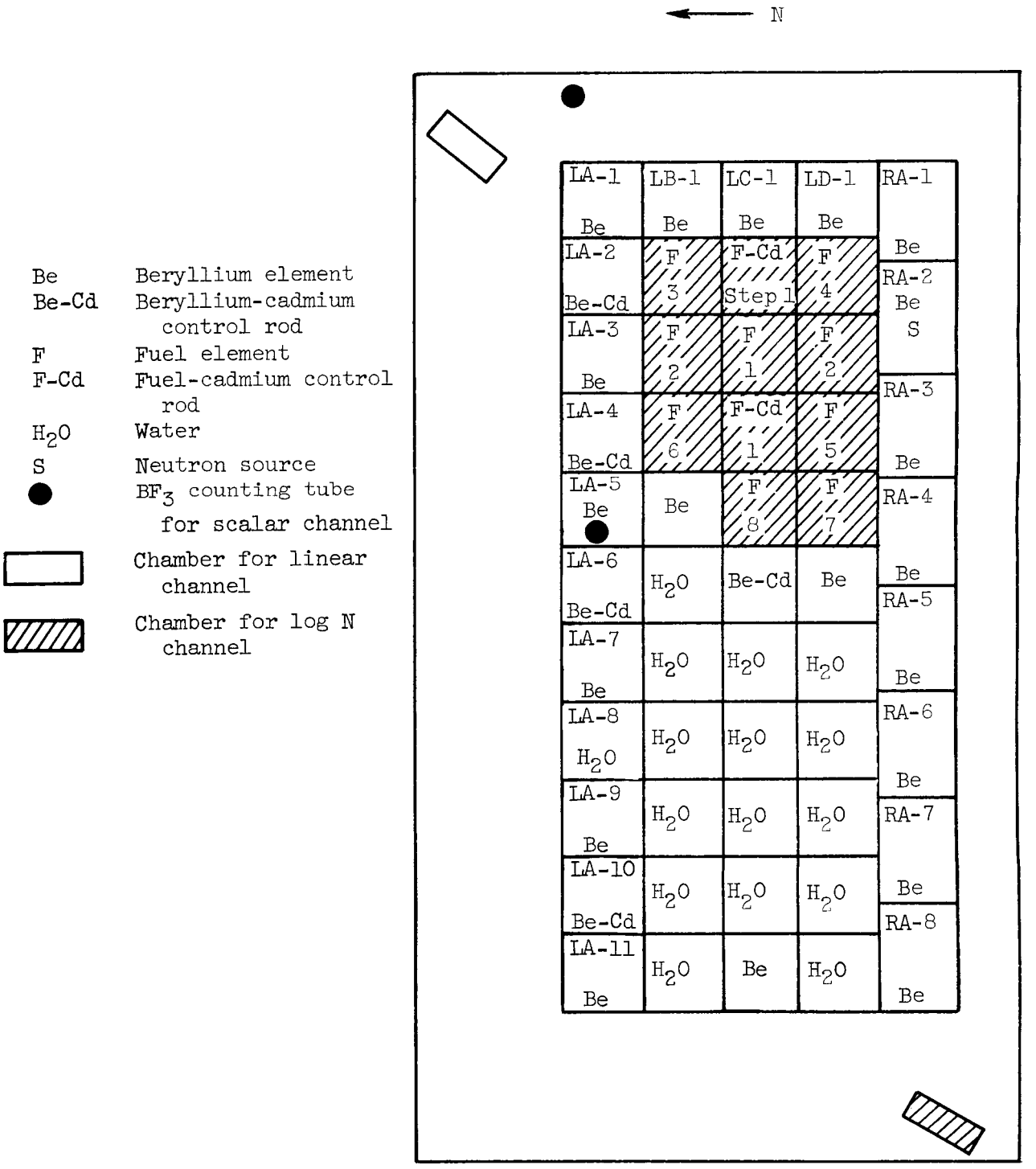

Figure 3. - Minimum critical core.

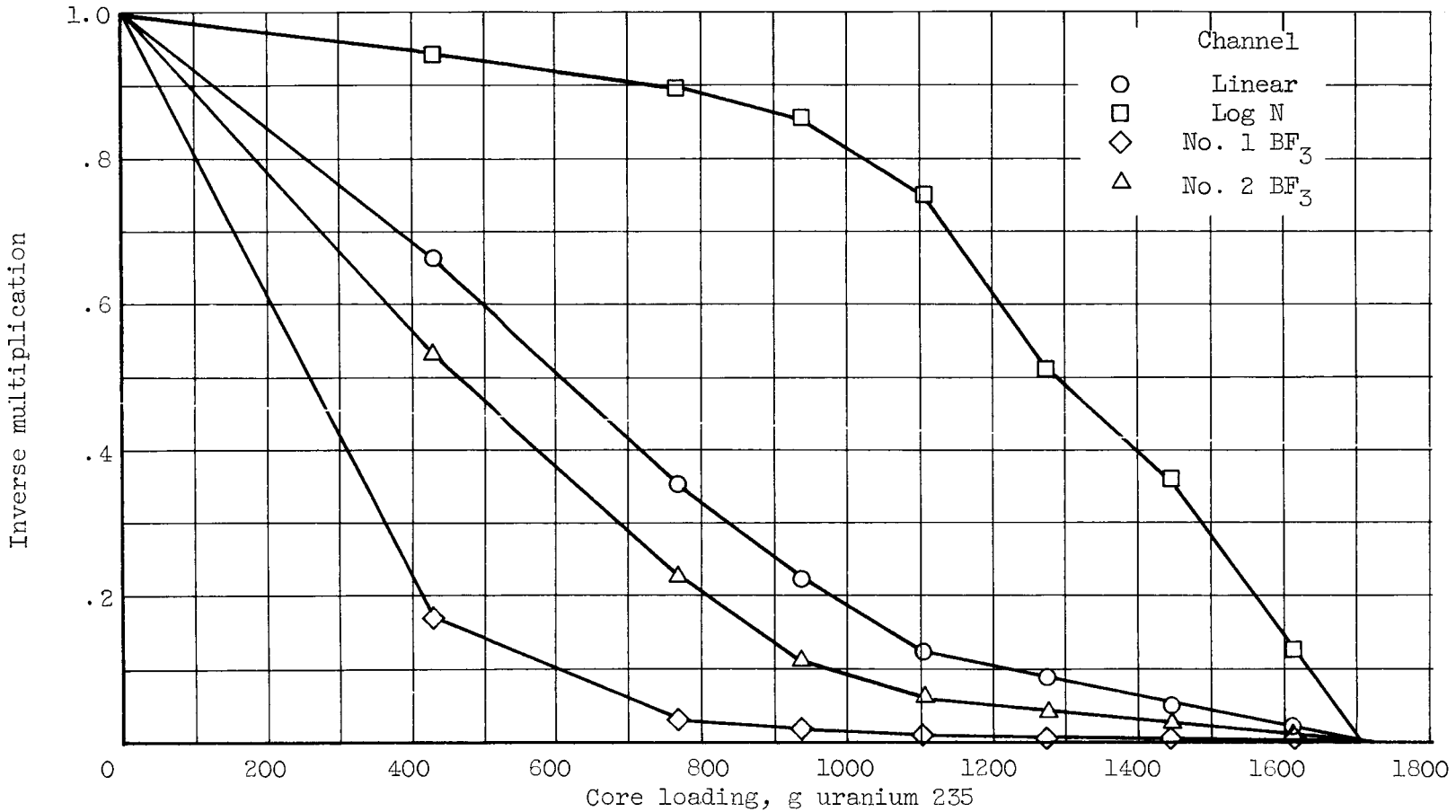

Figure 4. - Inverse multiplication plotted against core loading.

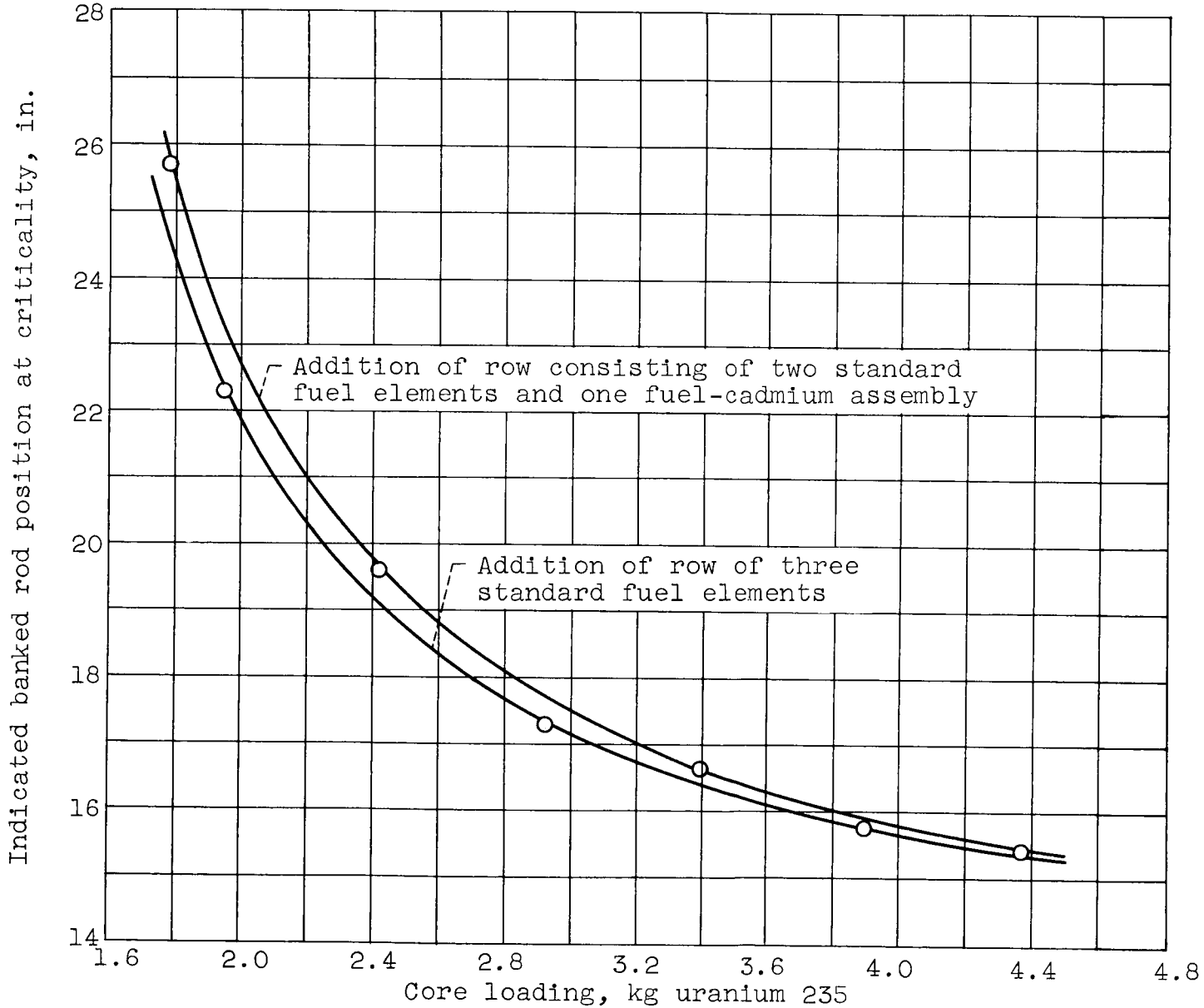

Figure 5. - Critical bank position plotted against core loading.

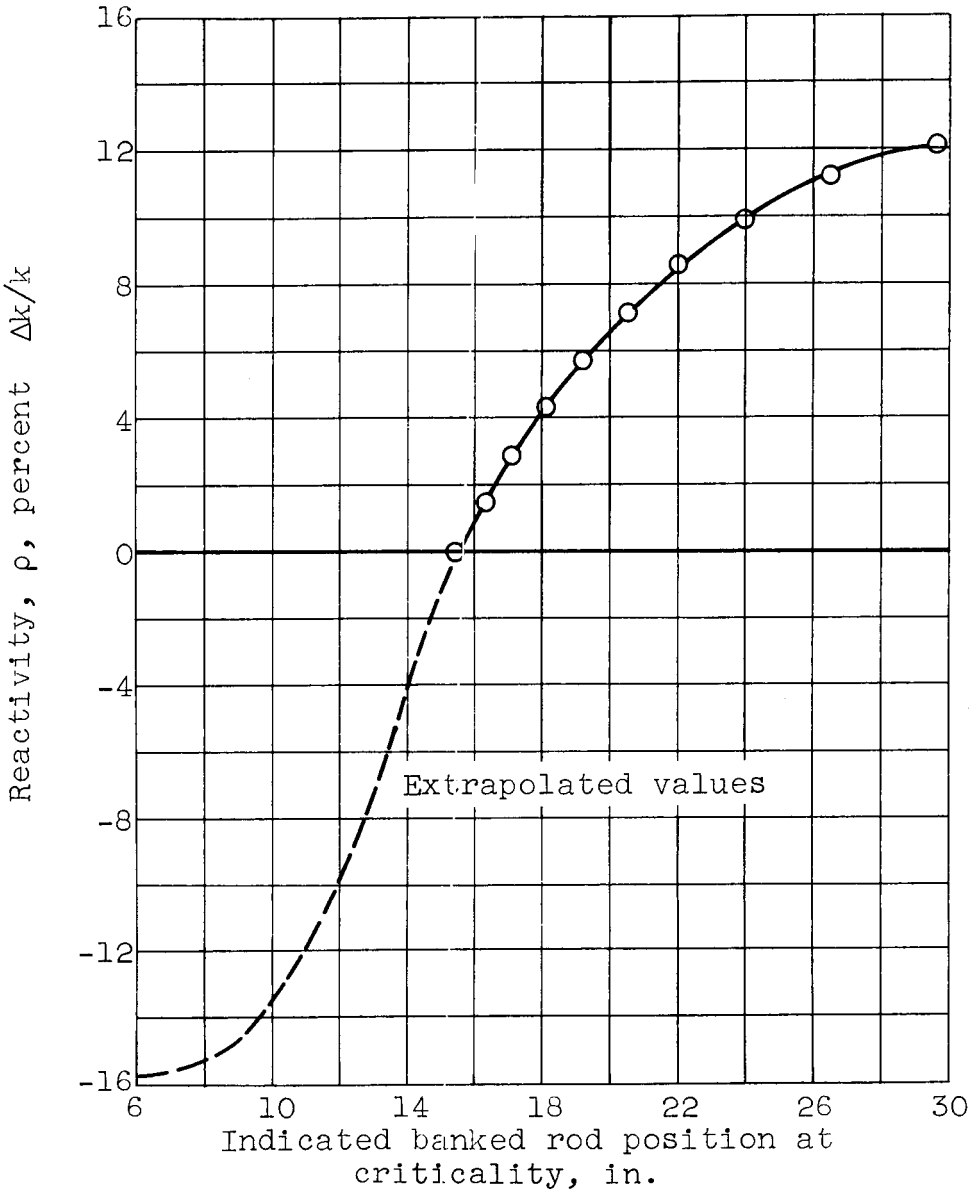

Figure 6. - Reactivity plotted against critical bank position.

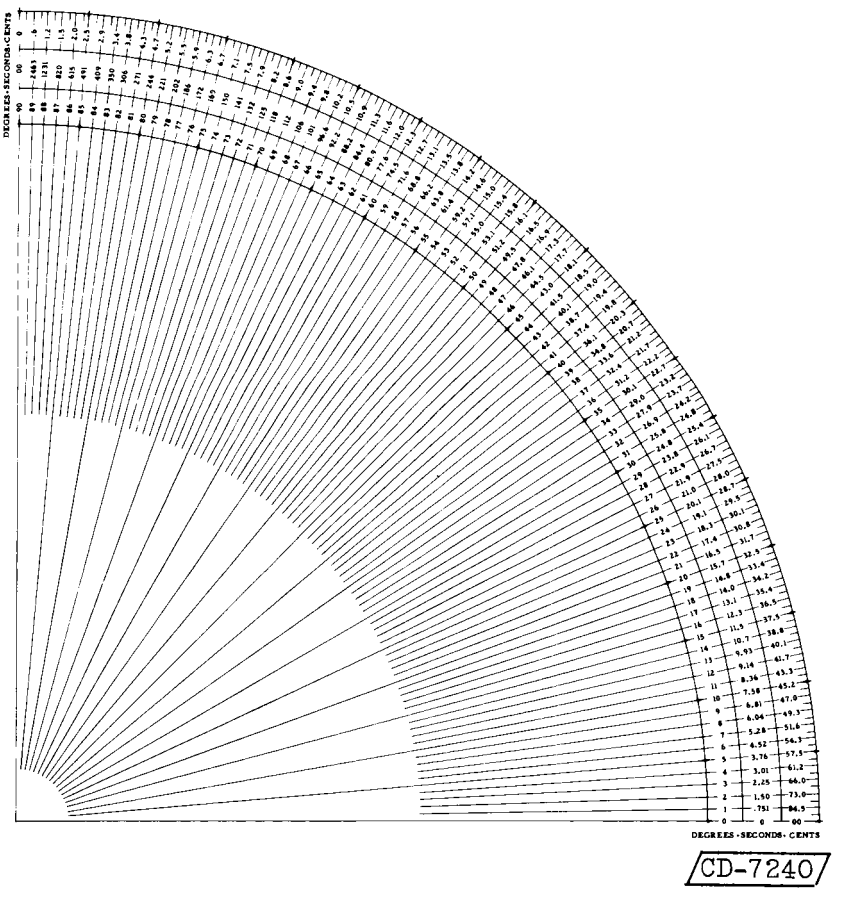

Figure 7. - Period protractor constructed of clear print attached to Lucite, used to determine reactivity from log N trace for rod bump-period measurements.

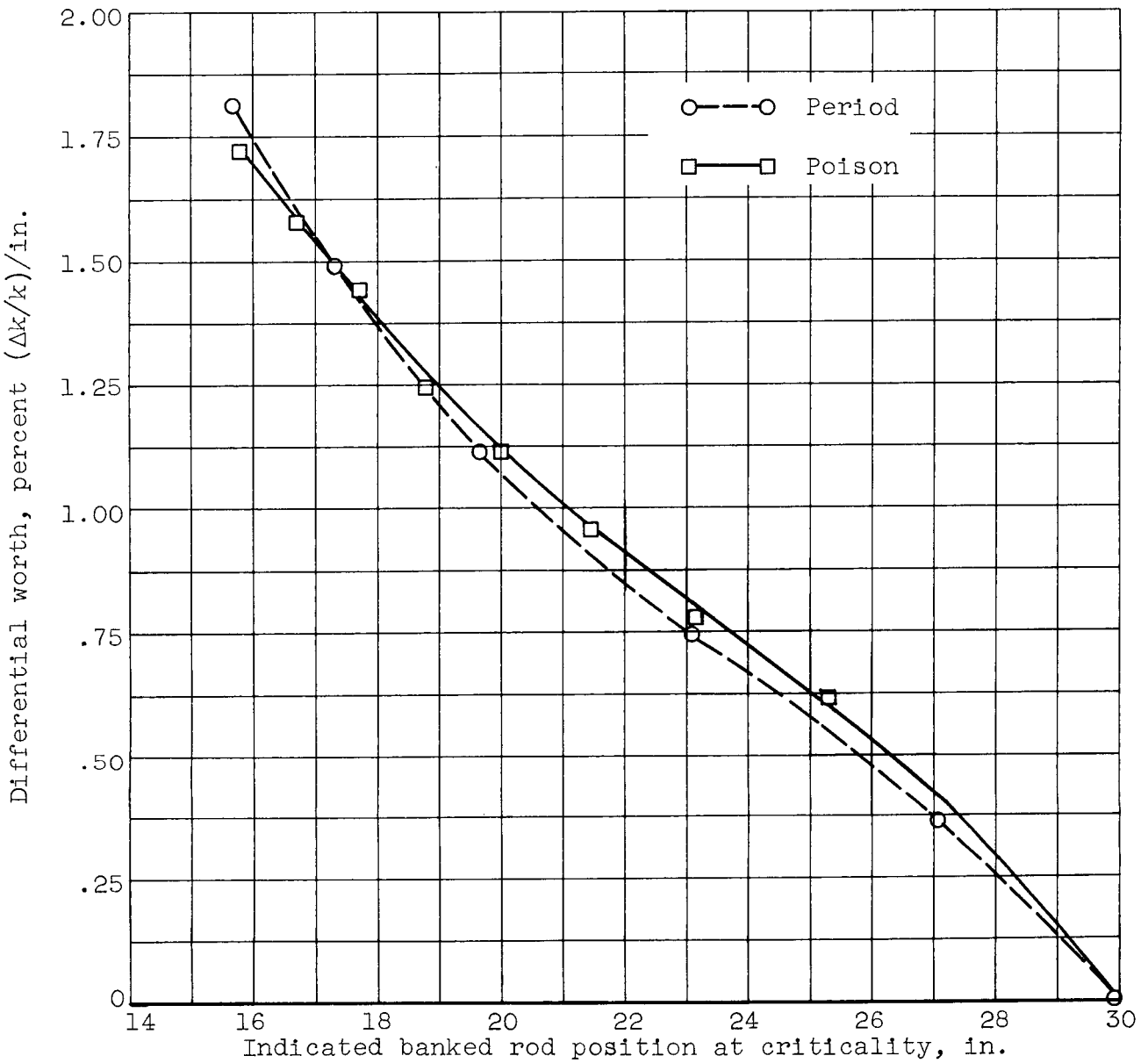

Figure 8. - Differential worth plotted against bank position.

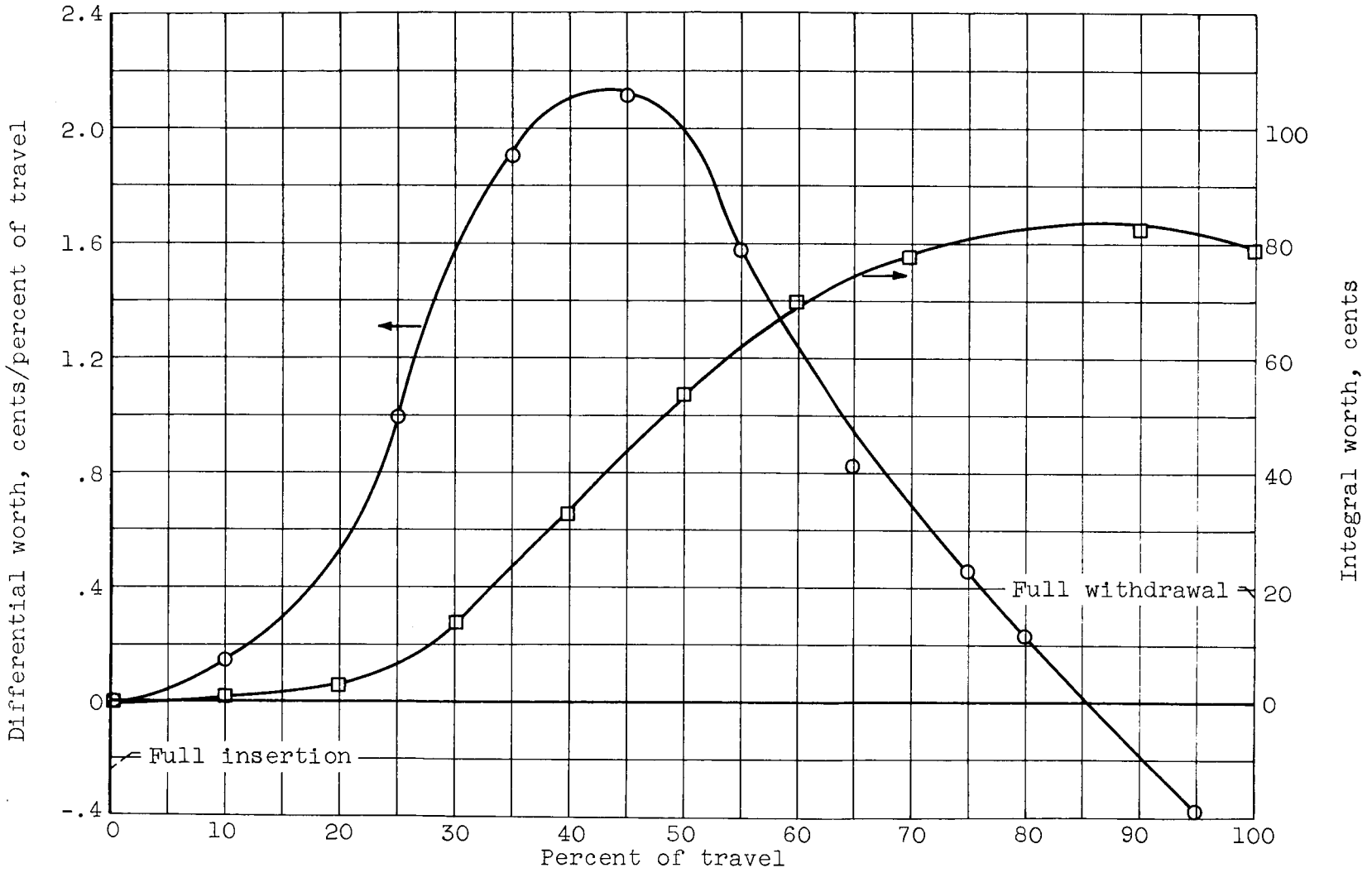

Figure 9. - Reactivity worth of regulating rod number 1. Fuel rod bank at 15.4 inches.

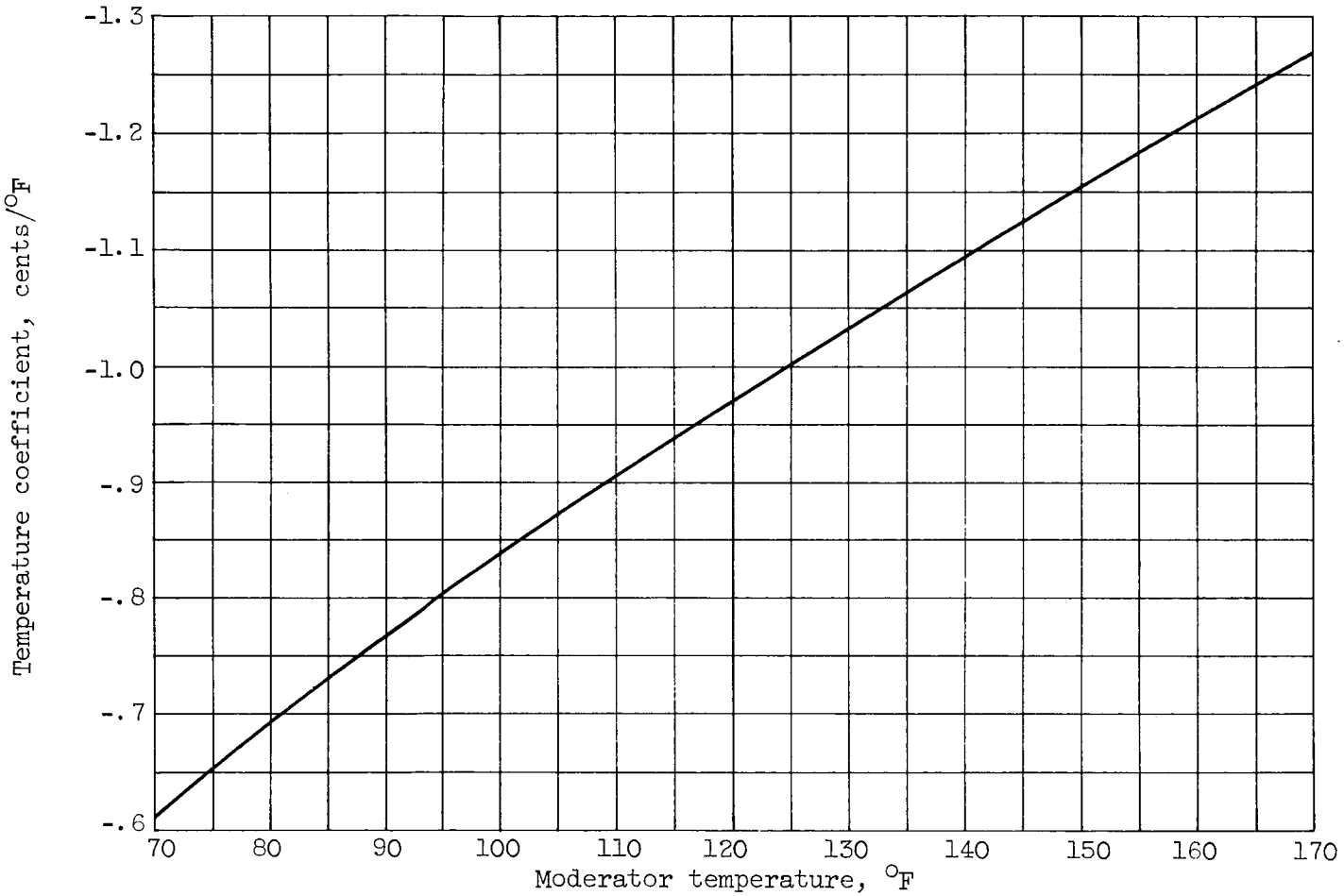

Figure 10. - Temperature coefficient plotted against temperature.

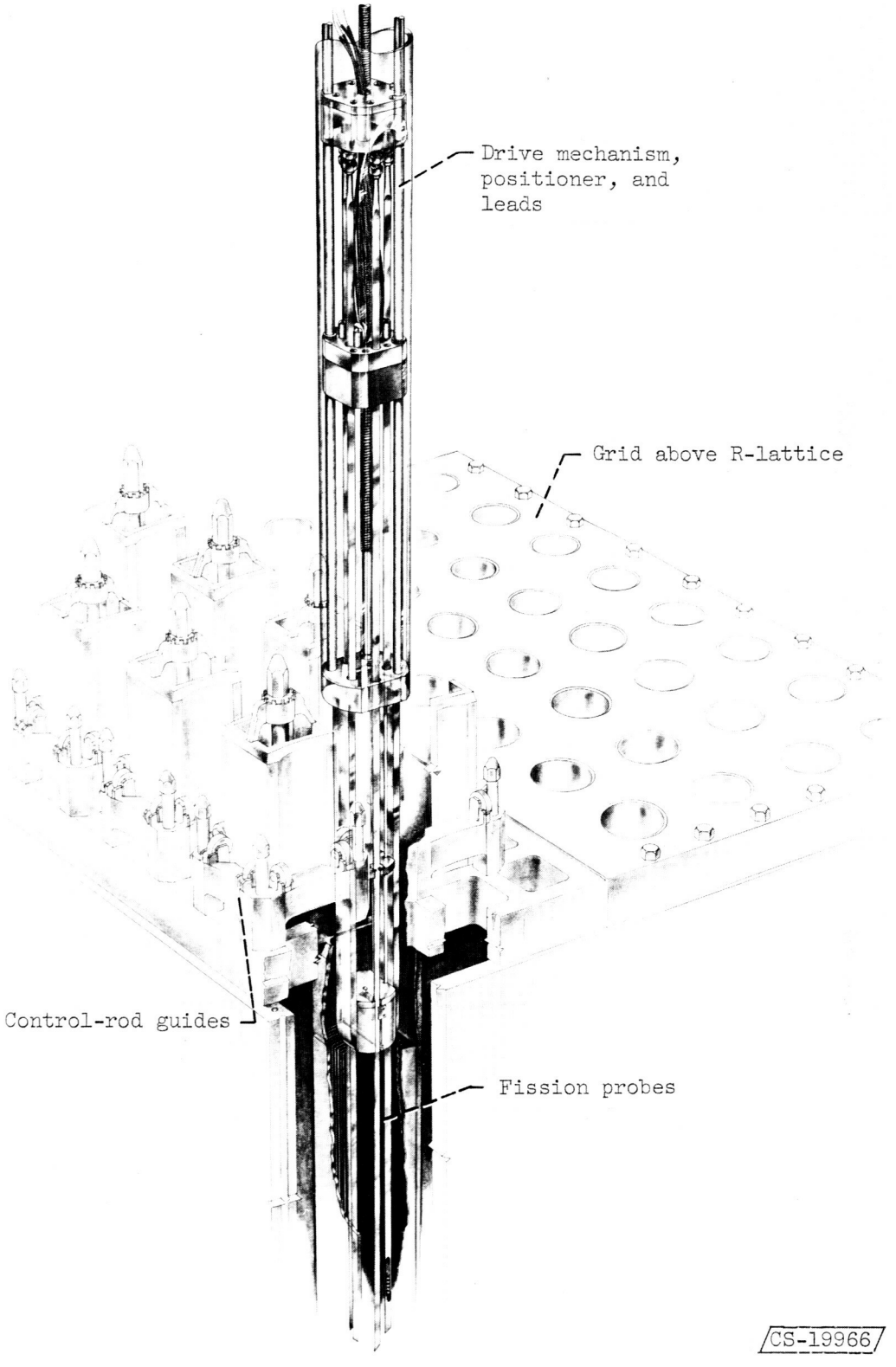

Figure 11. - Solid-state fission probe instrument (ref. 6).

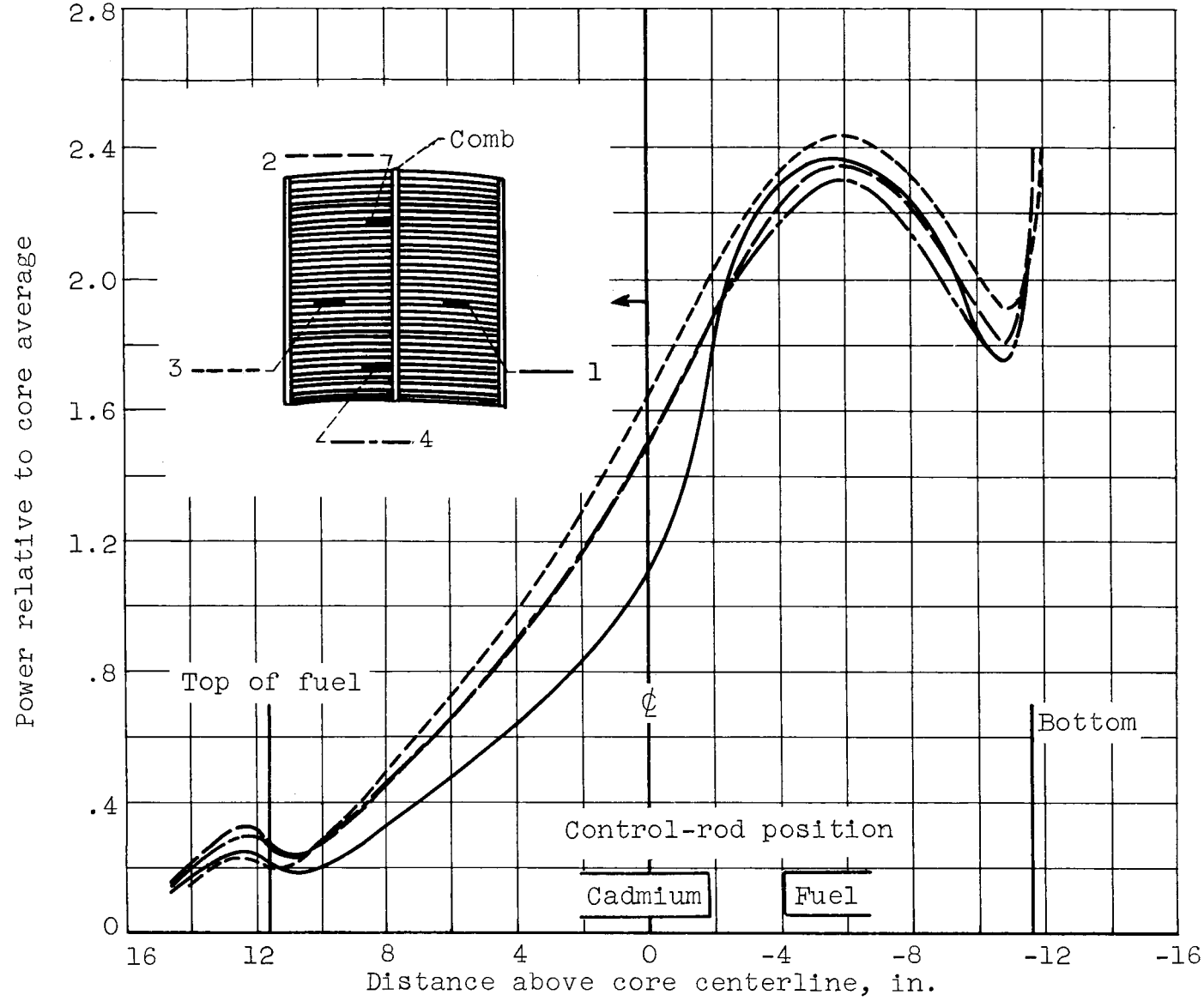

Figure 12. - Measured power distribution for individual probes. Element LB-6.

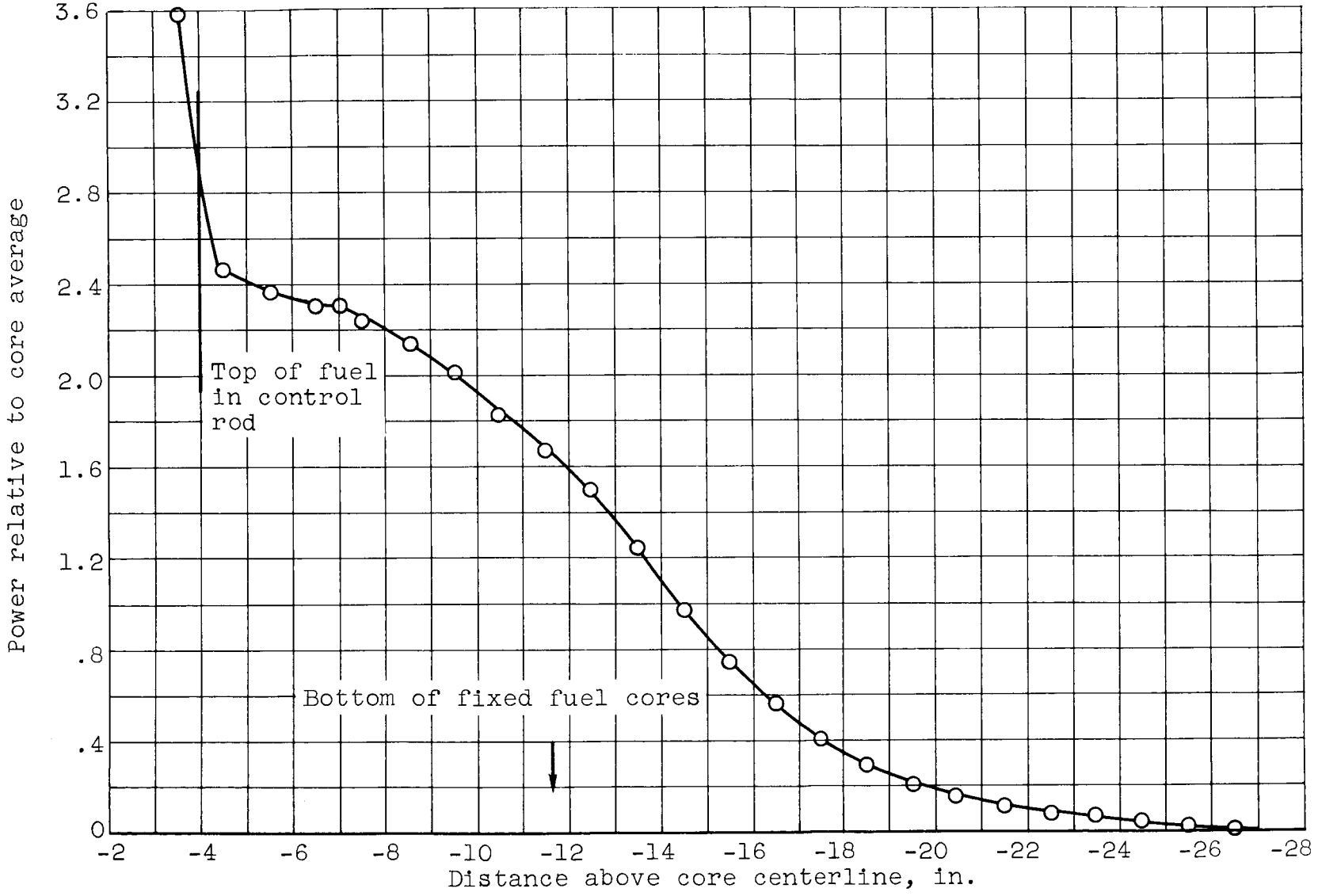

Figure 13. - Measured vertical power distribution. Element LC-6; rods at 15.4 inches.

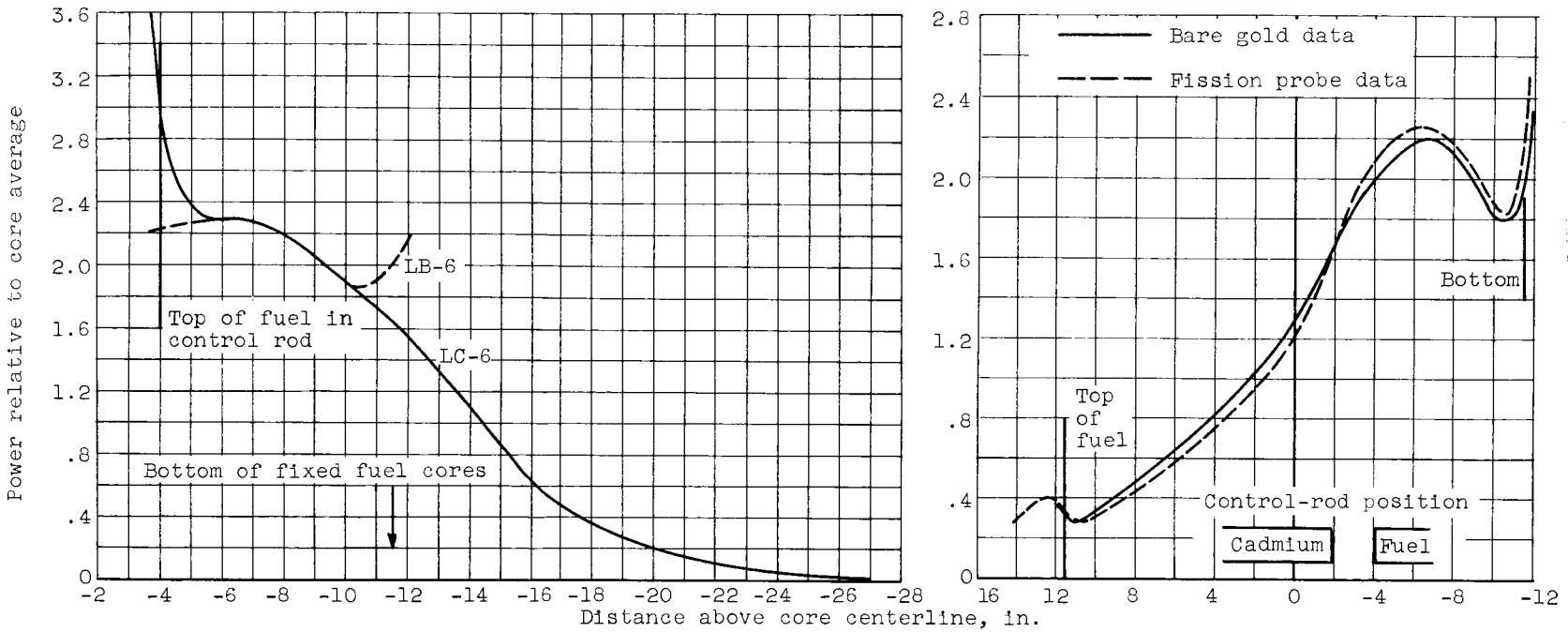

(a) Element LC-6.

(b) Element LD-6.

Figure 14. - Synthesized vertical power distribution. Rods at 15.4 inches.

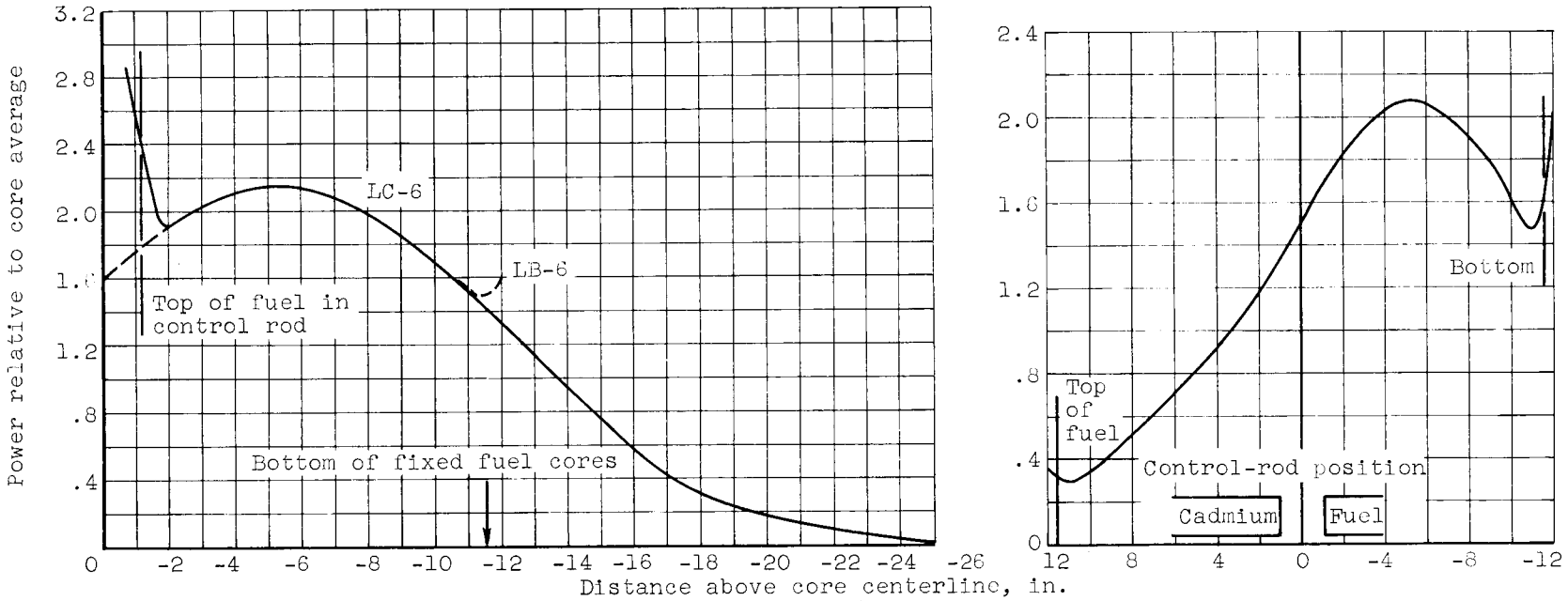

(a) Element LC-6.

(b) Element LD-6.

Figure 15. - Synthesized vertical power distribution. Rods at 18.3 inches.

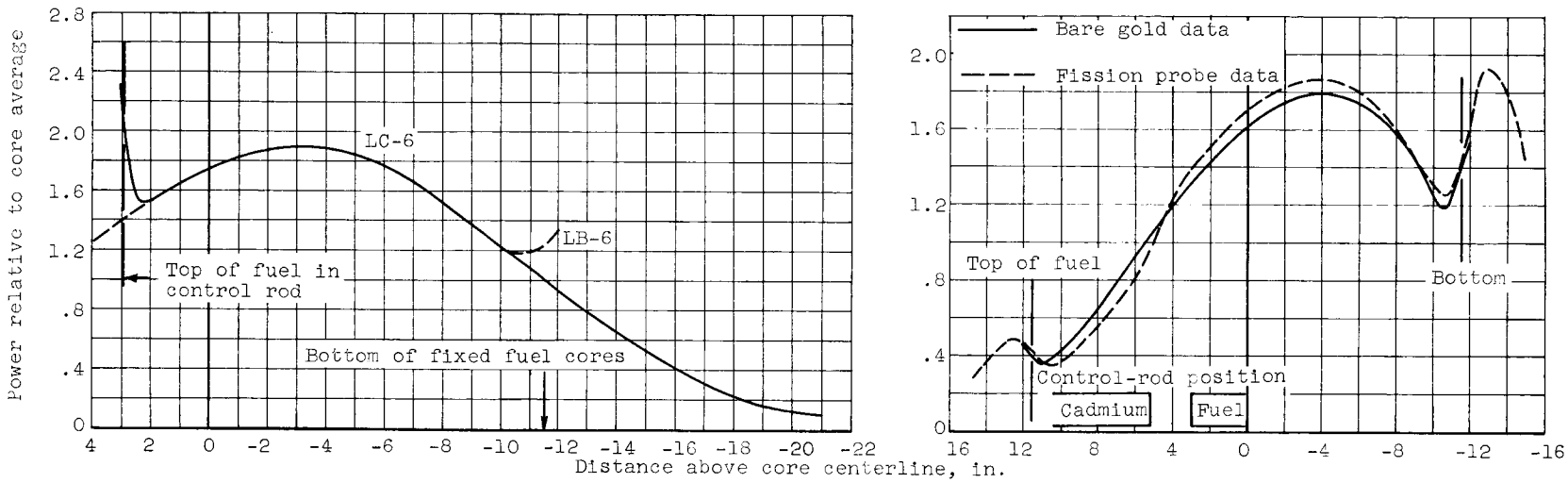

(a) Element LC-6.

(b) Element LD-6.

Figure 16. - Synthesized vertical power distribution. Rods at 22.3 inches.

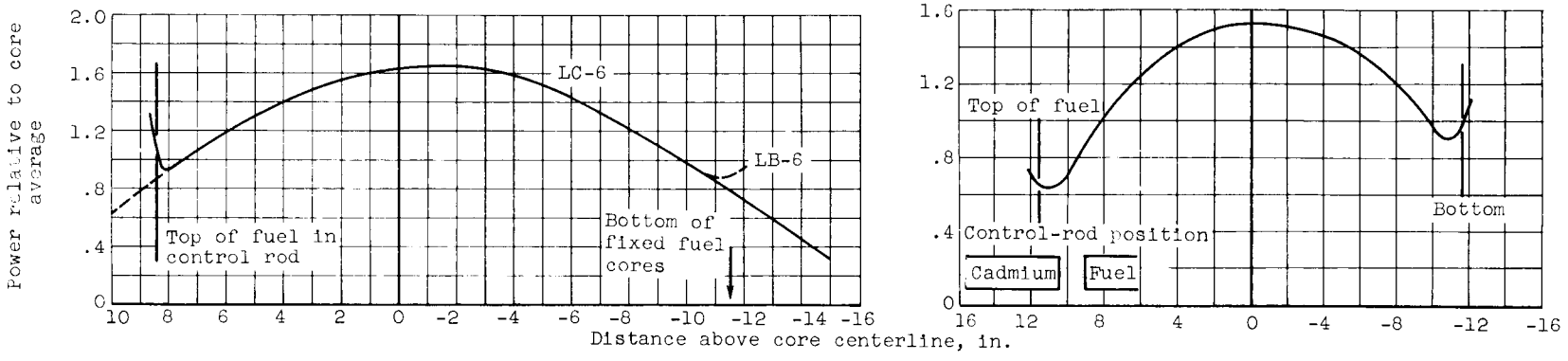

(a) Element LC-6.

(b) Element LD-6.

Figure 17. - Synthesized vertical power distribution. Rods at 27.8 inches.

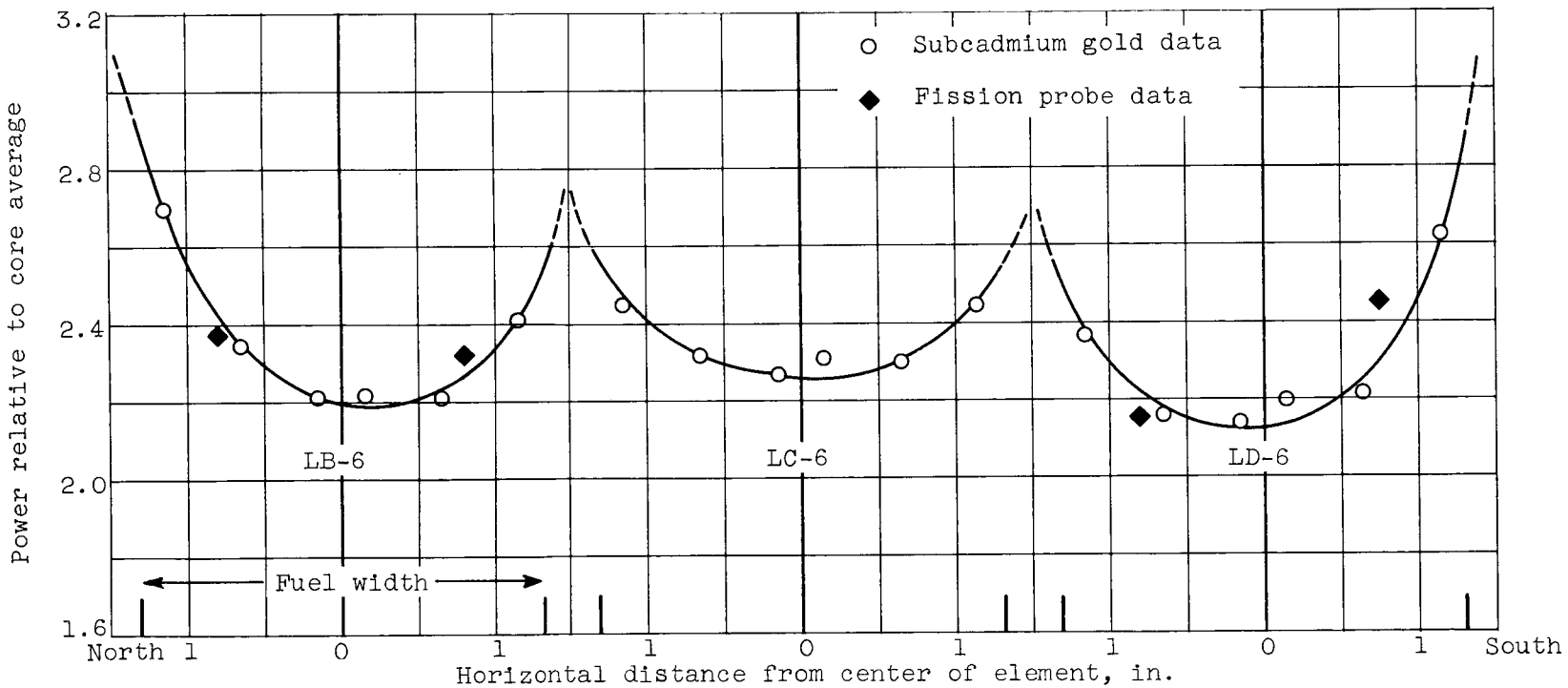

Figure 18. - North-south power distribution at -7 inches.

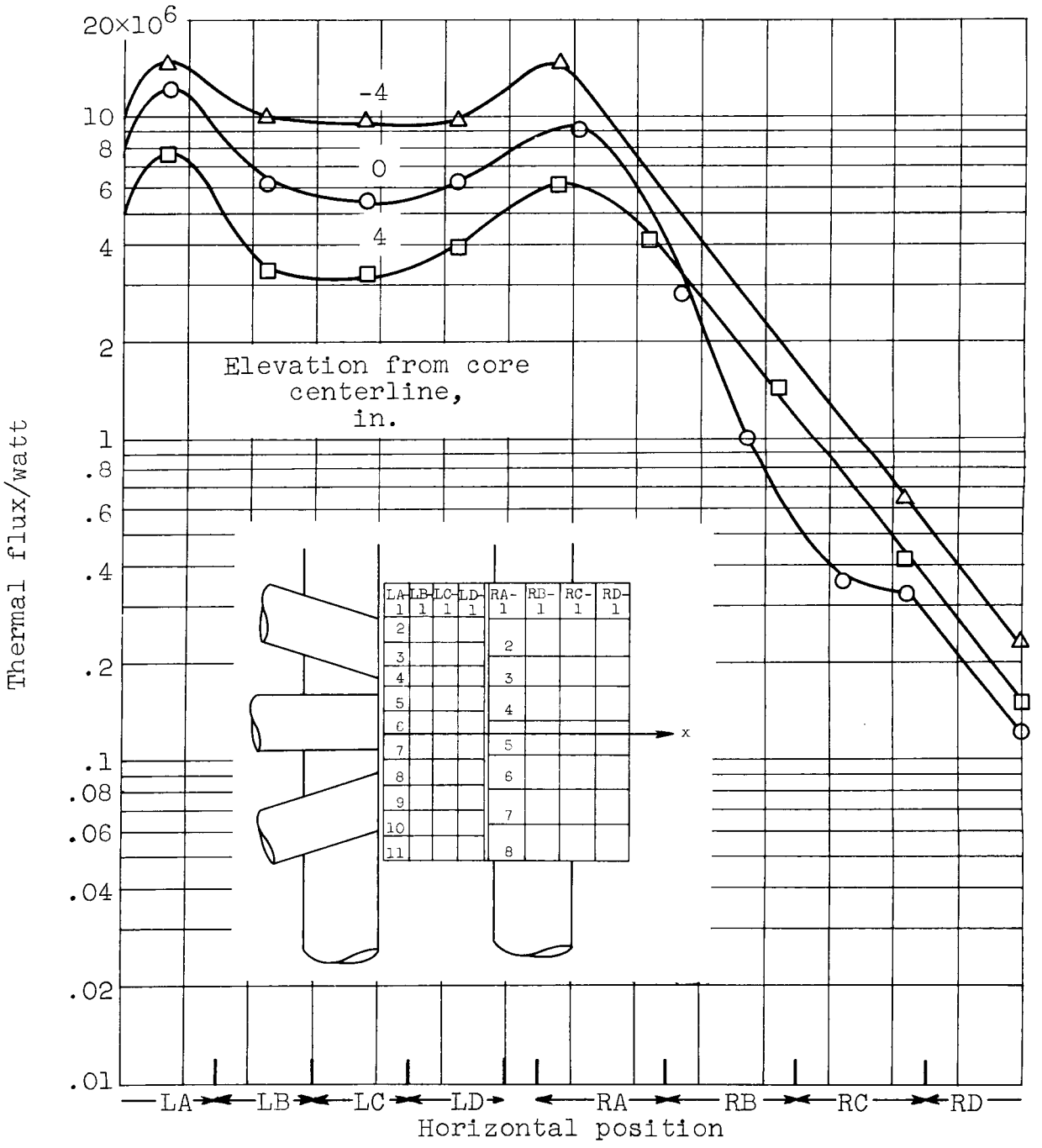

Figure 19. - Thermal flux distribution, north to south, core and reflector.

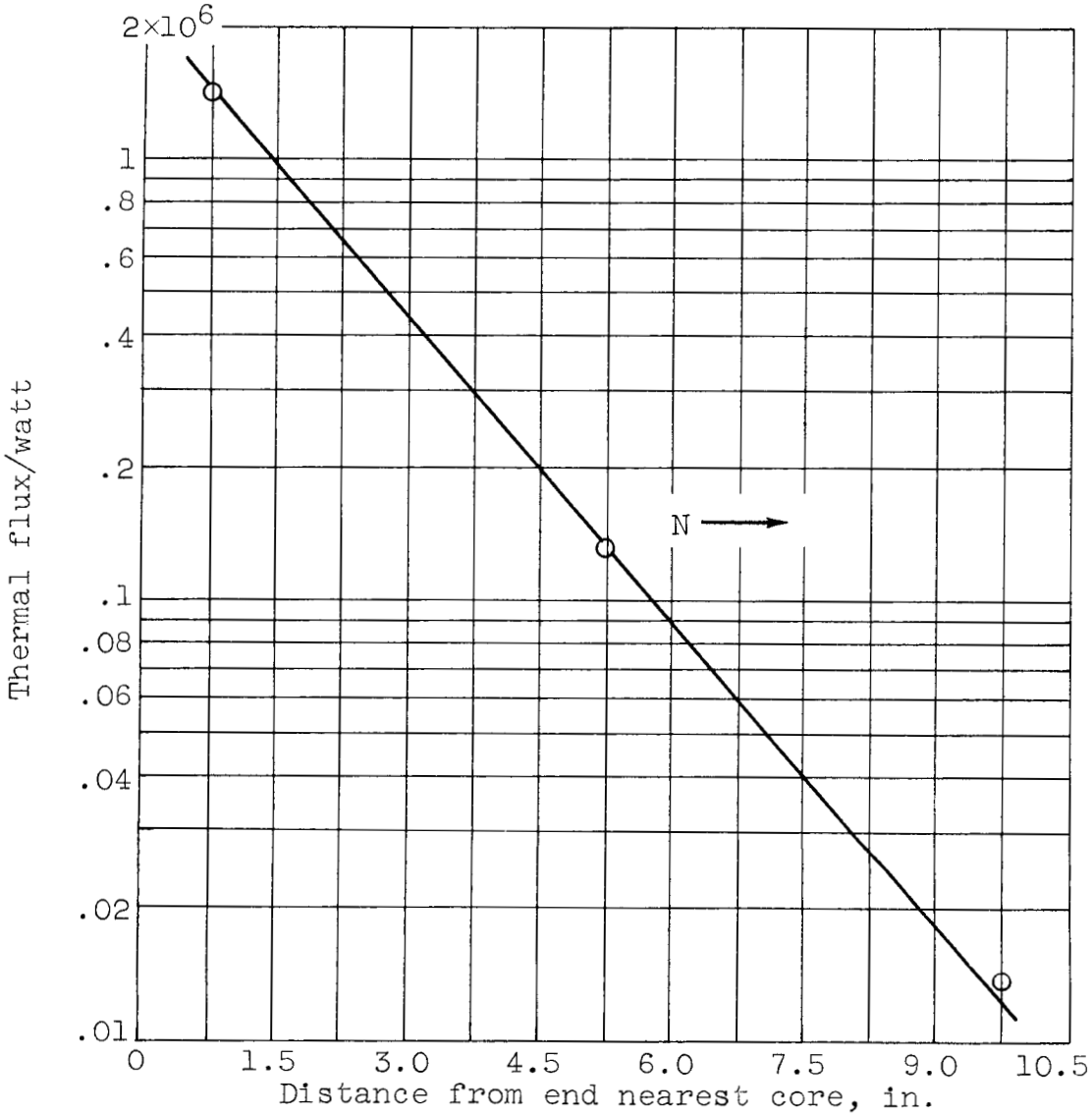

Figure 20. - Thermal flux along axis of HB-2.

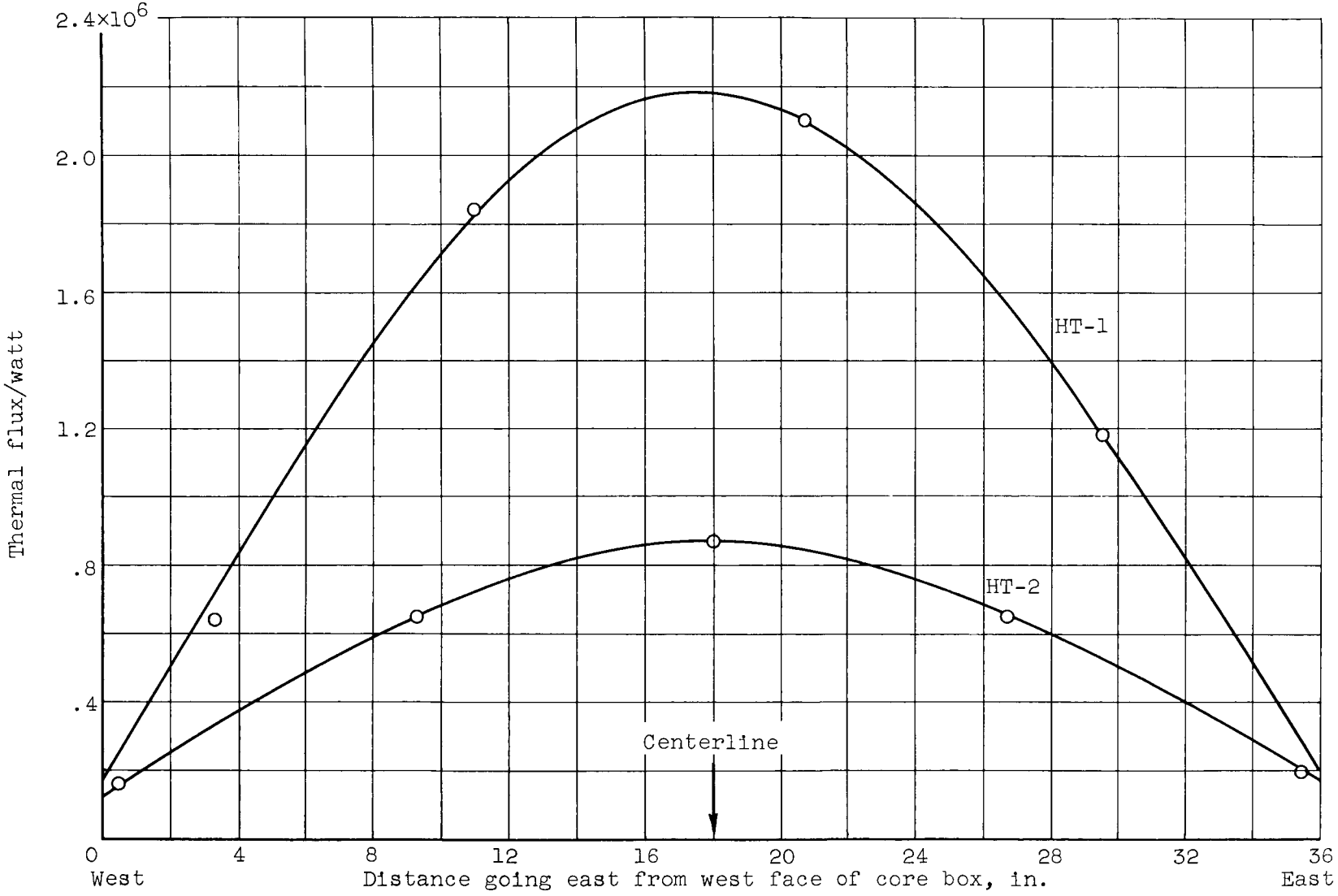

Figure 21. - Thermal flux along axes of horizontal through-holes.

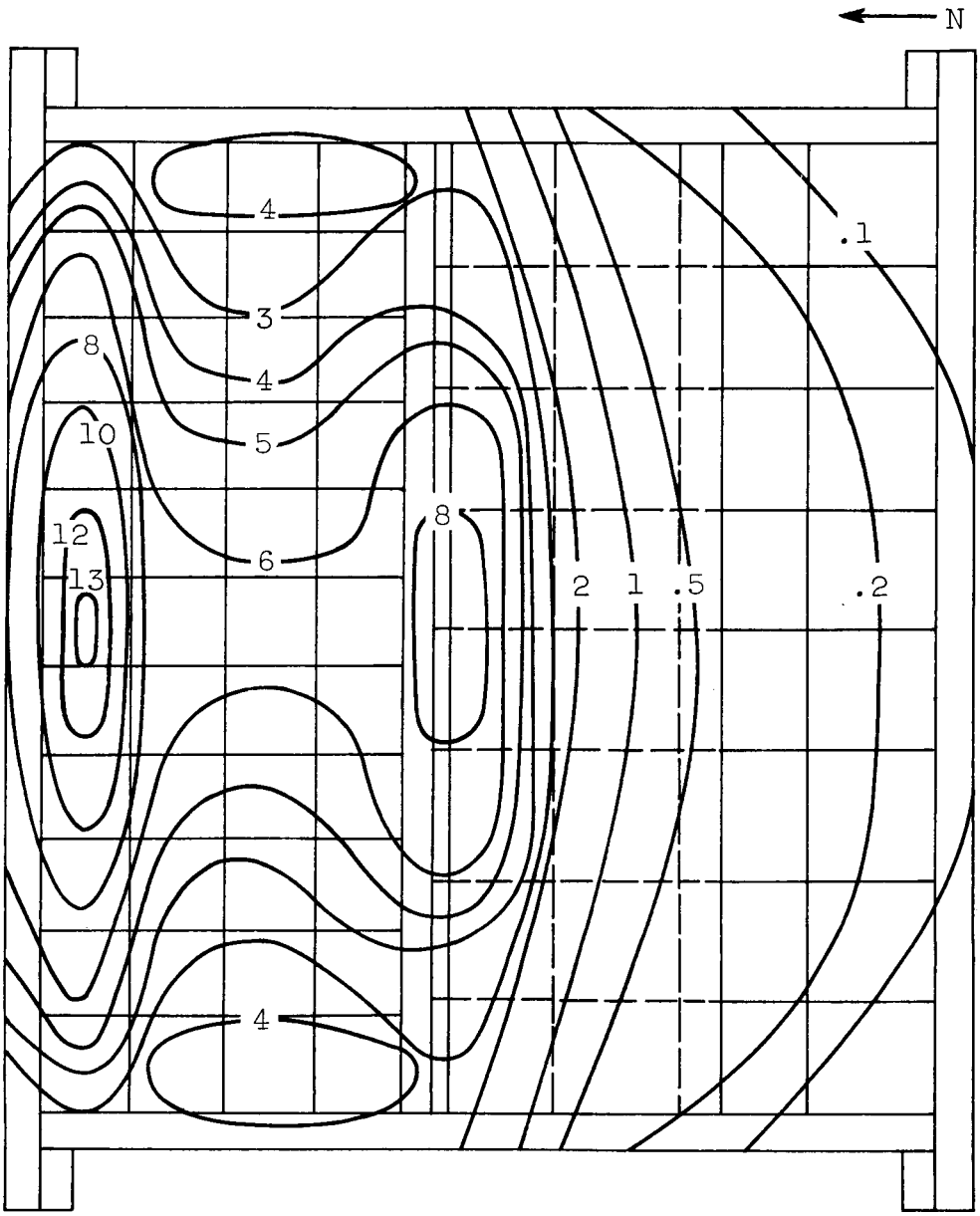

Figure 22. - Isoflux plot, core and reflector, at centerline elevation. Thermal flux per watt, $\varphi \times 10^{-6}$.

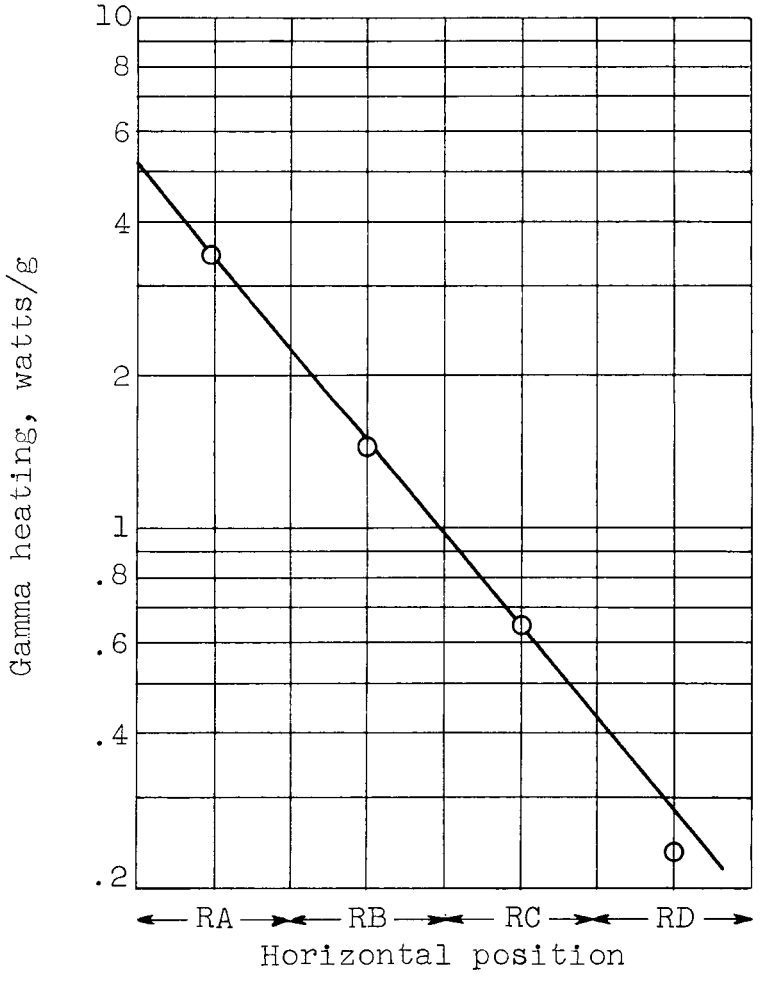

Figure 23. - Gamma heating along reflector lattice row number 4. Elevation $7\frac{1}{2}$ inches above core centerline.

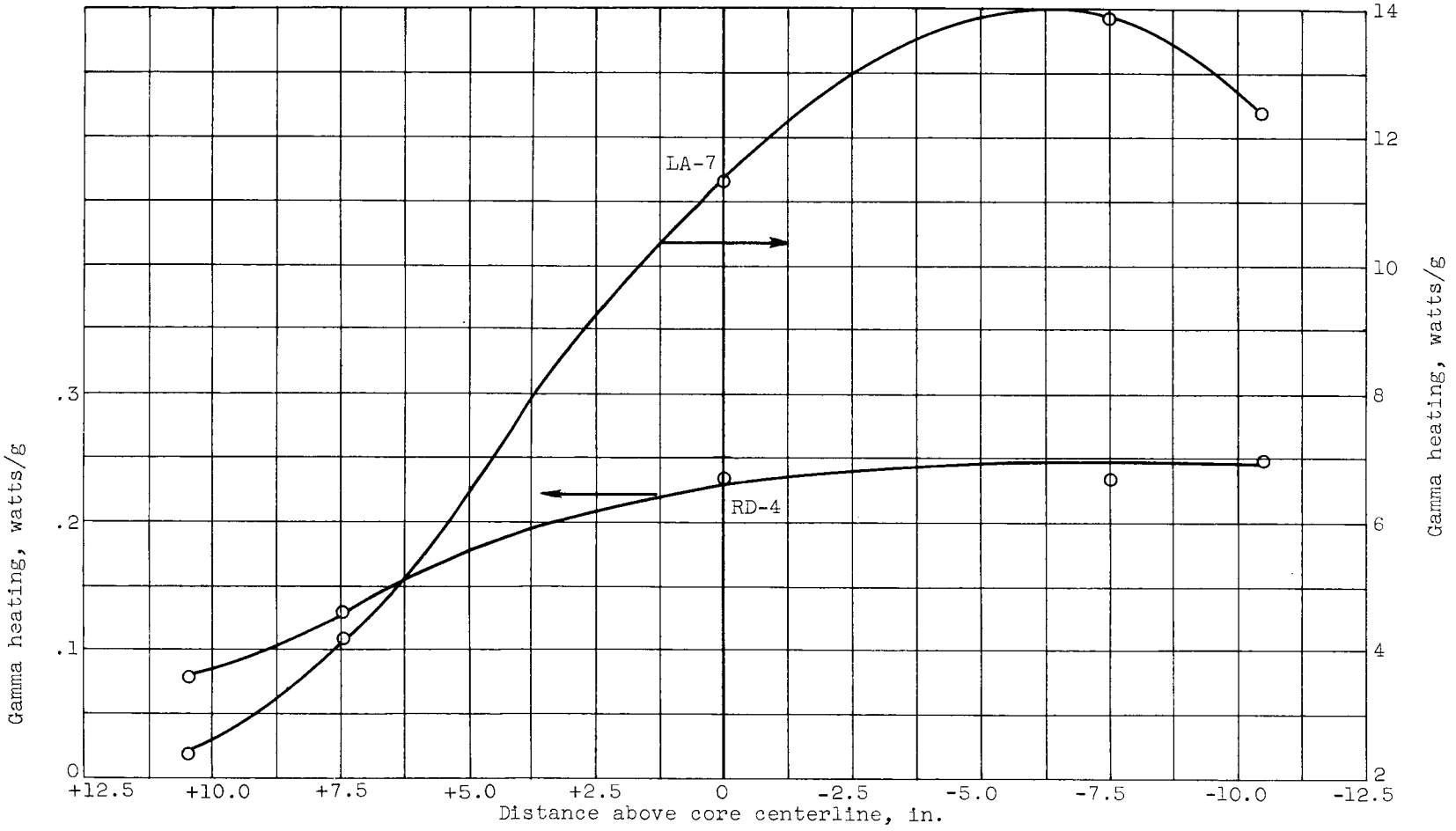

Figure 24. - Vertical gamma heating distribution using copper ion chambers.